SAND91-2575
Unlimited Release
Printed March 1992

Distribution
Category UC-126

Effects of Cavern Spacing and Pressure on Subsidence and Storage Losses for the US Strategic Petroleum Reserve

Brian Ehgartner
Underground Storage Technology Division
Sandia National Laboratories
Albuquerque, New Mexico

ABSTRACT

The effects of cavern spacing and operating pressure on surface subsidence and cavern storage losses were evaluated using the finite-element method. The base case for the two sensitivity studies was a typical SPR cavern. The predicted responses of the base case and those from the pressurization study compared quite closely to measured surface subsidence and oil pressurization rates. This provided credibility for the analyses and constitutive models used. Subsidence and cavern storage losses were found to be strongly influenced by cavern spacing and pressurization. The cavern spacing study showed 30 year subsidence predictions to increase from 4 in. for a single isolated cavern to 162 ft. for closely spaced caverns at 375 ft. The corresponding storage losses were effected to a lesser degree, ranging from 6 to 32 percent, respectively. The effects of cavern operating pressure were investigated by modeling surface oil pressures ranging from a maximum pressure of 1050 psi to zero. The resulting 30 year subsidence predictions ranged from 4 to 93 ft., while storage losses increased from 4 to 59 percent, respectively. The relationship between subsidence volume and losses in storage volume varied as cavern spacing and operating pressure deviated from the base case. However, for a typical SPR cavern subsidence volume is proportional to storage loss and when expressed in ft., subsidence is equal to the percentage of storage loss.

CONTENTS

FIGURES

TABLES

1.0 INTRODUCTION

The Strategic Petroleum Reserve (SPR) was created to reduce the vulnerability of the United States to interruptions by foreign oil suppliers. Approximately 670 million barrels (MMB) of crude oil are presently stored underground in salt domes at six sites located along the Gulf of Mexico. Most of the crude oil is stored in leached caverns.

Each cavern contains approximately 10 MMB of oil on top of approximately 1 MMB of brine. The caverns are accessed by one or more wells. Oil is removed by introducing brine into the bottom of the cavern. Pressures at the wellheads are determined by the location of the oil/brine interface. In this report, oil side or cavern operating pressure is defined as the oil pressure at the wellhead on the surface.

Cavern spacing and operating pressure are major design and operating parameters of current interest to the SPR given the possibility of expansion of existing sites or the development of new sites. Understanding the consequences of cavern operating pressure on storage loss and subsidence may also improve operations at existing cavern fields.

The finite-element method was used to evaluate the effects of cavern spacing and operating pressure on surface subsidence and cavern volume losses. Surface subsidence is important given the proximity of several of the sites to sea level and its potential impact on well casings, surface piping, and other structures that support oil withdrawal and storage. Storage losses have primarily an economic impact as the capacity and operational life of the facility are affected. Storage losses and surface subsidence are inter-related and time-dependent due to creep of the salt. Volume losses of the cavern are manifested as surface subsidence. Cavern stability is also evaluated for each of the analyses performed.

Cavern spacing and operating pressure were evaluated in separate studies. Each parameter was varied over a large range which included

the base case-- a typical SPR Cavern. A typical SPR cavern was defined as 2000 ft. high, 170 ft. in diameter, located 2500 ft. below the surface. The typical or baseline cavern was spaced at 750 ft. and operated at a oil side pressure of 680 psi. The finite-element model was 2-D axisymmetric with a stratigraphy of surface overburden, caprock, and salt, similar to that found at West Hackberry. The time-dependent response of a field of oil filled cylindrical caverns was simulated for 30 years.

In the cavern spacing study, the distance between the caverns was varied at 375, 750, 1500, and 3000 ft. The spacings represent a range from very closely spaced caverns to nearly isolated single caverns. The cavern operating pressure was held constant at the baseline value of 680 psi in the cavern spacing study. The pressurization study used the baseline cavern spacing of 750 ft. and performed calculations for oil side pressures of 0, 300, 680, and 1050 psi. An operating pressure of 1050 psi represents the maximum allowable for most wells at West Hackberry, whereas a 0 psi oil side pressure is required during a workover. Workovers are periodically required for maintenance of the access wells and surveys of the caverns.

The finite-element model, constitutive models and properties, analytic results, comparison of predicted results to field measurements, and conclusions are discussed in the following chapters.

2.0 FINITE-ELEMENT MODEL

Figure 1 shows the 4 different finite-element meshes used in the axisymmetric analyses of the caverns. Due to a high density of elements, the meshing is partly obscure in some areas. Each mesh consisted of 520 elements and 571 nodes. Mesh refinement was based on a series of 1 dimensional finite-element calculations that modeled a horizontal slice of the cavern. The meshing study varied the number, gradation, and aspect ratios of the elements.

Cavern spacing was modeled by adjusting the mesh width to equal one-half of the cavern spacing. The spacings of 375, 750, 1500, and 3000 ft. translate into pillar-to-cavern diameter (P/D) ratios of 0.39, 1.78, 4.56, and 10.1, where the pillar width (P) is based on the expected diameter (D) of 270 ft. after five complete fill and drawdown cycles (SPR, 1987). The design criteria for SPR caverns constrains the P/D ratio to a minimum of 1.78 (SPR, 1987). The mesh for the 750 ft. spacing was used in all 4 of the pressure calculations.

A "rollered" boundary condition along the right edge of the mesh approximates an infinite field of evenly spaced caverns. Rollers do not allow normal displacements at the boundary, but freely permit tangential displacements. In an infinite field of evenly spaced caverns, these boundary conditions exist at points located equal distance from the caverns to form planes of geometric symmetry. The planes form a honeycomb or polygon pattern around the caverns in the field. In the model, the polygonal shape of the true boundary is approximated as circular due to axisymmetric rotation of the mesh about the centerline of the cavern. Therefore, the approximation improves as the number of caverns in an actual pattern increases. Loading symmetry is also assumed, implying that all the caverns in a field are constructed at the same time and have identical pressure histories. In reality, cavern fields are of finite extent, therefore the modeling better approximates subsidence and cavern deformations in the middle of the field rather than at the edges of a cavern field where deformations may be limited due to the lack of neighboring caverns.

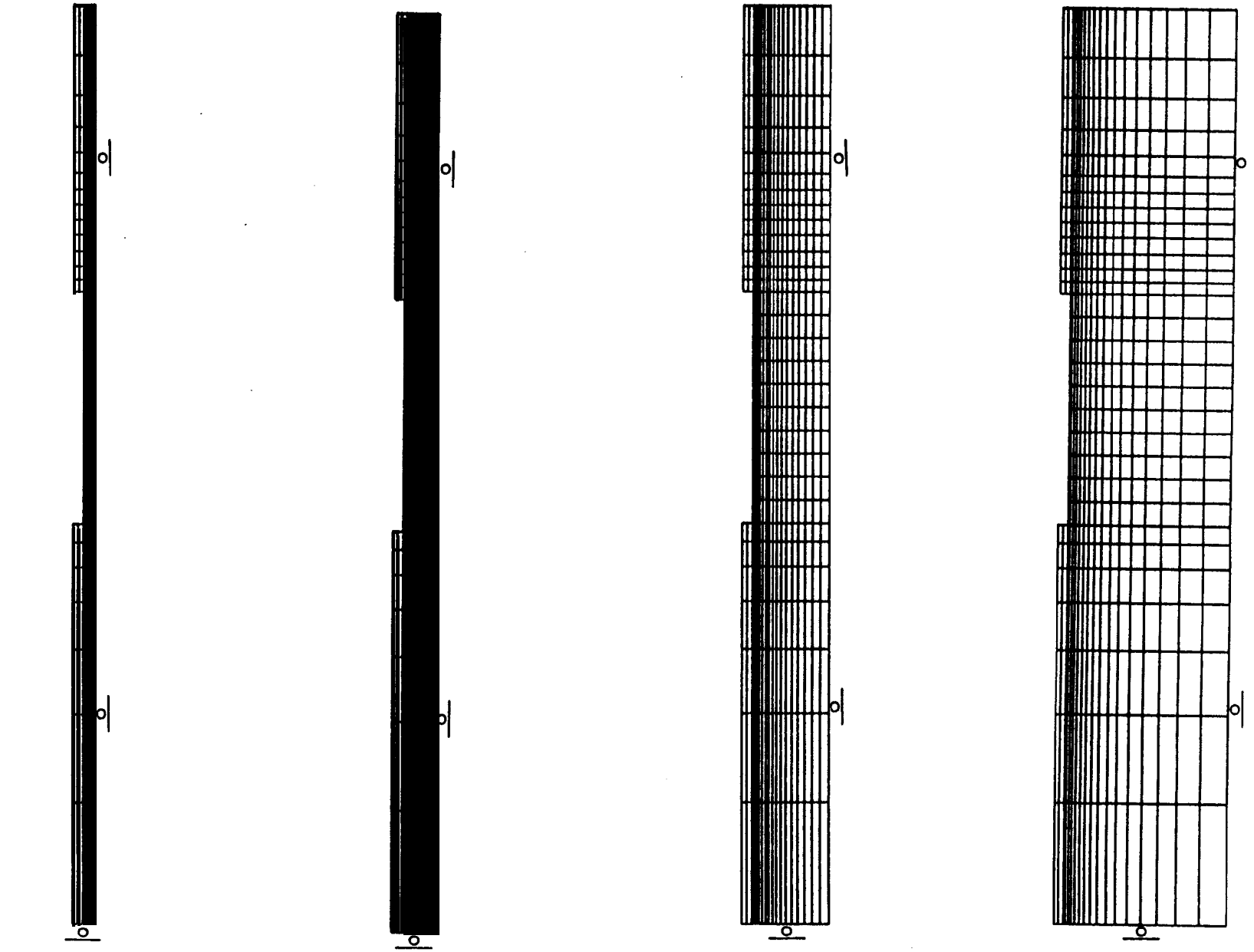

Figure 1. Axisymmetric Finite Element Meshes of Caverns Spaced at 375, 750, 1500, and 3000 ft.

The initial stresses in the model were based on gravity loading of the overburden, caprock, and salt. The stratigraphy consisted of 1600 ft. of overburden, 400 ft. of caprock, and 5500 ft. of salt. The insitu stress state of the salt was set to hydrostatic based on the weight of the salt and overlying rock. The cavern was located 500 ft. below the bottom of the caprock.

Mining of the caverns was simulated as instantaneous with an internal fluid (crude oil) pressure was applied to the cavern walls. The weight of the oil resulted in a pressure gradient (0.37 psi/ft) along the length of the cavern, where the applied pressure was simply the sum of the weight of the oil and well pressure.

The oil/brine interface was assumed to be at the bottom of the cavern or 4500 ft. below the surface. Assuming a brine pressure gradient of 0.52 psi/ft, the baseline oil side pressure was 680 psi. This pressure is defined as the baseline pressure, as such it was used in all the cavern spacing calculations. Oil side pressures of 0, 300, 680, and 1050 psi were simulated in the pressurization study. The oil side pressure remained constant over the 30 years simulated in all of the analyses. In reality, well pressures increase with time due to creep and thermal effects. As a result, they are periodically bled to keep them below the maximum operating pressure specified for a cavern. The periodic bleed or depressurization results in transient creep. Such details were not simulated in these analyses. However, the baseline oil side pressure (680 psi) is at the low end of the typical operating range. This will help to account for the transient effects not modeled.

Cavern enlargement or leaching due to fluid transfers was not simulated over the 30 year period. SPR drawdowns have been small in scale and limited during the past 12 years. To some extent, the effects of future drawdowns on subsidence and volume losses will be mitigated as the stresses surrounding the older caverns will be relaxed due to creep and the removal of salt in older caverns will not result in transients as large as those in newly formed caverns. Therefore it may not be necessary to discretely model increases in cavern size for long-term performance predictions. However, to accurately model early cavern

performance it may be necessary, particularly since it typically takes 2 to 3 years to develop a cavern and fill it with oil.

The surface temperature was assumed constant at 83°F, and an insitu temperature gradient of 0.012°F/ft of depth was applied to the stratigraphy. This resulted in a temperature of 137°F at the bottom of the cavern. Local temperature variations in the salt due to heat transfer between the salt and cavern fluids were not modeled. Both temperature and stress control the creep rate as discussed below.

3.0 CONSTITUTIVE MODELS AND PROPERTIES

The constitutive models and properties used to represent the mechanical behavior of the salt host rock and its caprock and overburden are discussed along with the finite-element computer code used for the analyses.

3.1 Modeling of Salt

The mechanical behavior of the salt was represented by the Munson-Dawson creep model. The model is state-of-art in predicting salt behavior using a first principles approach. The model was developed for the Waste Isolation Pilot Plant (WIPP) Project and has been used to model a wide variety of underground structures and openings in salt at that site (Ehgartner 1990, 1991). The WIPP, located in southeastern New Mexico, is a room and pillar facility designed for underground disposal of transuranic wastes in bedded salt.

The model is presently being validated with underground data from the WIPP and the validation exercises thus far show good to excellent agreement of predicted room closures with underground measurements in Rooms B, D, G, and the South Drift of the WIPP (Munson, Fossum, and Senseny, 1989a,b; Munson and DeVries, 1990). Preliminary comparisons between predicted and measured shaft closures in the Air Intake Shaft at the WIPP show excellent agreement (Munson, et. al.,1992).

The model is a Multimechanism Steady State Workhardening/Recovery Model as originally developed by Munson and Dawson (1979) and later modified to provide a more descriptive transient strain function (Munson, Fossum, and Senseny, 1989a,b). The model incorporates the Tresca flow potential and is based on micromechanistic concepts using a deformation mechanism map (Munson, 1979). The mechanism map defines regions of stress and temperature in which a unique deformation mechanism controls or dominates steady-state creep. The model identifies three steady-state mechanisms: Mechanism 1 (dislocation climb) dominates at high

temperatures and low stresses; Mechanism 2 (undefined) dominates at low temperatures and stresses; and Mechanism 3 (dislocation glide) dominates at high stresses at all temperatures. The steady state strain rates for Mechanisms 1 and 2 are equal to:

$$A\, e^{(-Q/RT)}\, s^{n},$$

where A is a constant, Q is the activation energy, T is the absolute temperature, R is the universal gas constant (1.987 cal/mol-°K), s is the generalized stress, and n is the stress exponent. The basic form of the equation for Mechanism 3 is similar to above, except it is preceded by a Heaviside step function with an argument of $s - sig_o$, where sig_o is the stress limit of the dislocation slip mechanism. The form of the creep law for steady state Mechanisms 1 and 2 is similar to that used in previous analyses for both the Waste Isolation Pilot Plant (WIPP) and the SPR (Krieg, 1984).

Transient creep is included in the model through a function composed of a workhardening branch, an equilibrium branch, and a recovery branch. The details of this component and the steady-state component of creep are discussed by Munson, Fossum, and Senseny (1989a).

The salt properties in the analyses were based on steady state creep tests of West Hackberry salt (Wawersik and Zeuch, 1984) to define Mechanism 2. The properties required for Mechanisms 1 and 3, and for the transient portion of the model were not available for West Hackberry salt, therefore WIPP properties were used as needed. West Hackberry salt creeps at a steady state rate of approximately 80% of WIPP salt. The WIPP properties are from an extensive reevaluation of the WIPP data bases (Munson, Fossum, and Senseny 1989a,b). Table 1 lists the elastic, steady state creep, and transient creep properties of salt used in the analyses. Previous analytical studies (Preece, 1987a,b) used a creep model which accounted for only steady state creep and required an empirical reduction of the elastic modulus to better match field

measurements. No such empirical adjustments are necessary for the creep model used in the present study.

Table 1
Mechanical Properties of Salt*

Elastic Properties			
Poisson's Ratio	0.25		
Modulus of Elasticity (E)	31.0 **GPa**		
Creep Properties			
Steady-state Mechanism 1		Steady-state Mechanism 2	
A_1	8.386 E22 **/s**	A_2	1.290 El2 **/s**
Q_1	25000 **cal/mol**	Q_2	12000 **cal/mol**
$"_1$	5.5	$"_2$	4.9
Steady-state Mechanism 3		Transient Creep	
B_1	6.086 E6 **/s**	m	3.0
B_2	3.034 E-2 **/s**	K	6.275 E5
sig_o	20.57 **MPa**	c	0.009198 **/T**
q	5.335 E3	a	-17.37
		b	-7.738
		d	1.05

* For a complete definition of the above parameters see Munson, Fossum, and Senseny, **1990a**.

3.2 Xodeling of Caprock and Overburden

The caprock and overburden were modeled as elastic materials using the properties listed in Table 2. The modulus and Poisson's ratio were obtained from standard triaxial strength tests on laboratory size samples from the SPR. In order to account for fracturing of the caprock and other scale dependencies, the modulus of elasticity for the caprock used in the analyses and reported in Table 2 is the laboratory value divided by 10. The modulus for the overburden, typically a clayey sand, was not reduced from the laboratory measurements as scale effects are assumed to be negligible. Values of density are based on research by Todd (1991).

Table 2
Mechanical Properties of Caprock and Overburden

	Caprock	Overburden
Poisson's Ratio	0.288*	0.33"
Modulus of Elasticity (MPa)	709*	43.1**
Density (g/cc)	2.5	1.874

* Preece and Foley, 1984
** Acres, 1986

3.3 Finite-Element Code

The SPECTROM-32 code (RE/SPEC, 1989), version 3.07, was used to perform the simulations. The code is a two-dimensional finite-element thermomechanical stress analysis program written to solve nonlinear, time-dependent rock mechanics problems.

4.0 ANALYTICAL RESULTS OF CAVERN SPACING STUDY

The effects of cavern spacing on surface subsidence and cavern storage or volume losses are discussed below.

4.1 Effects on Subsidence

Figure 2 plots cavern spacing vs. the predicted subsidence at 30 years for the 4 analyses. A third or fifth degree polynomial was used in this and all remaining figures to provide interpolation between results. Subsidence is strongly influenced by cavern spacing as evidenced by the logarithmic plot which shows the 30 year subsidence to range from 0.3 ft. for caverns spaced at 3000 ft. to 163 ft. for caverns spaced at 375 ft. For all 4 spacings modeled, no significant subsidence trough was formed at the ground surface. This may be an artifact of the model because the calculations simulate an infinite number of evenly spaced caverns of identical geometries and operating pressures. However, uniform surface subsidence was also predicted for the larger cavern spacings which tend to represent single isolated caverns.

For isolated caverns, the development of a subsidence trough is a function of the operating pressure. Figure 3 shows subsidence profiles at the ground surface and along the top of the salt for an unpressurized isolated cavern (nearest neighbor over 4 miles away) at 10 years. This calculation was done aside from the 4 cases described above, but used the same material properties and cavern geometry. A zero oil side pressure was applied. The vertical displacement is exaggerated 500 times to show the development of the trough at both the surface and top of salt. The maximum subsidence at the top of the salt does not occur directly over the top of the cavern. This is a result of the flow pattern established by the salt, where the dominant flow (and corresponding largest cavern deformation) is near the bottom of the cavern wall. The flow of salt into this area draws upon pillar salt, which results in a subsidence at the top of the salt offset from the cavern centerline.

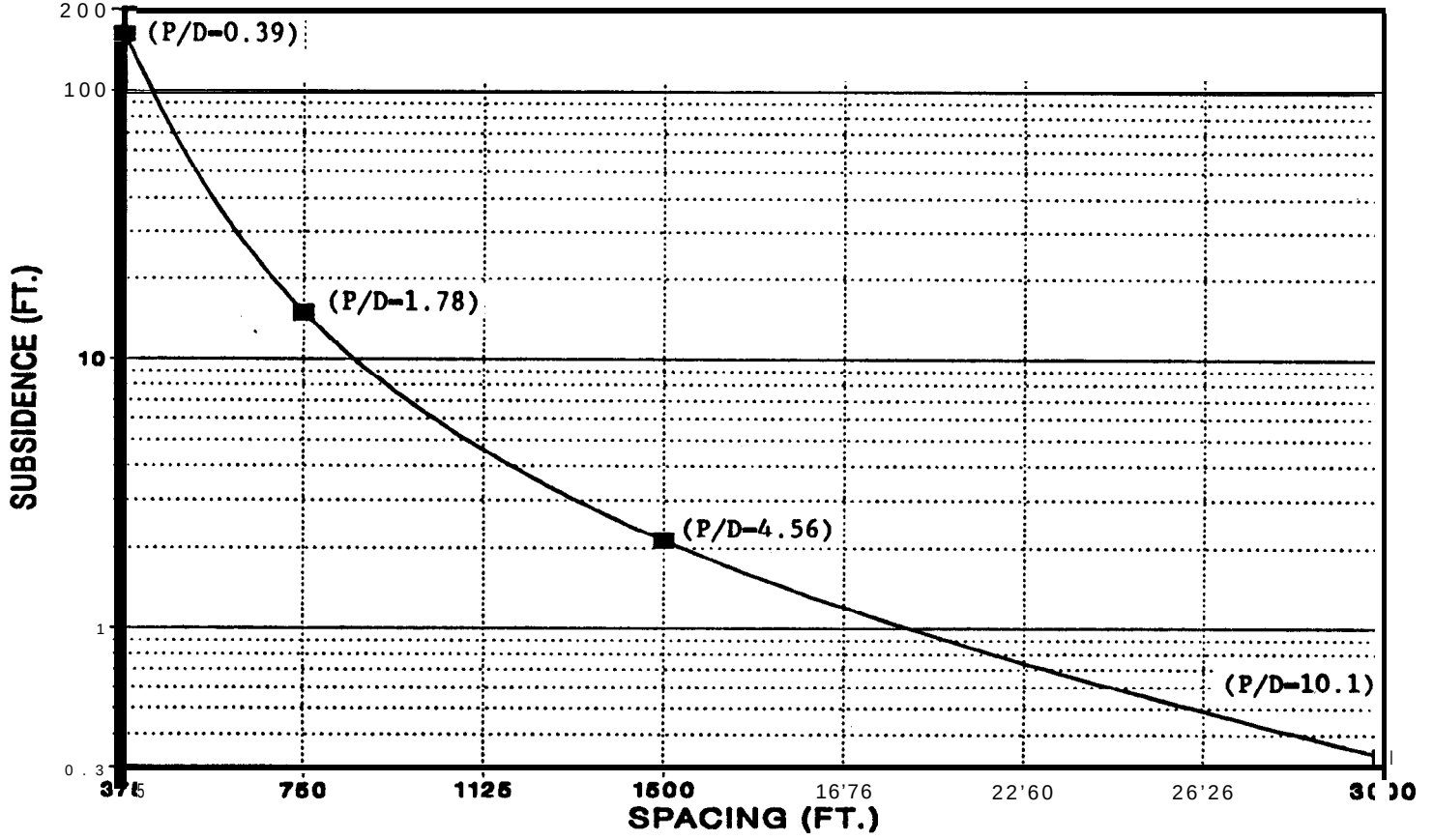

Figure 2. Subsidence at 30 Years vs. Cavern Spacing. (Semi-Log Plot).

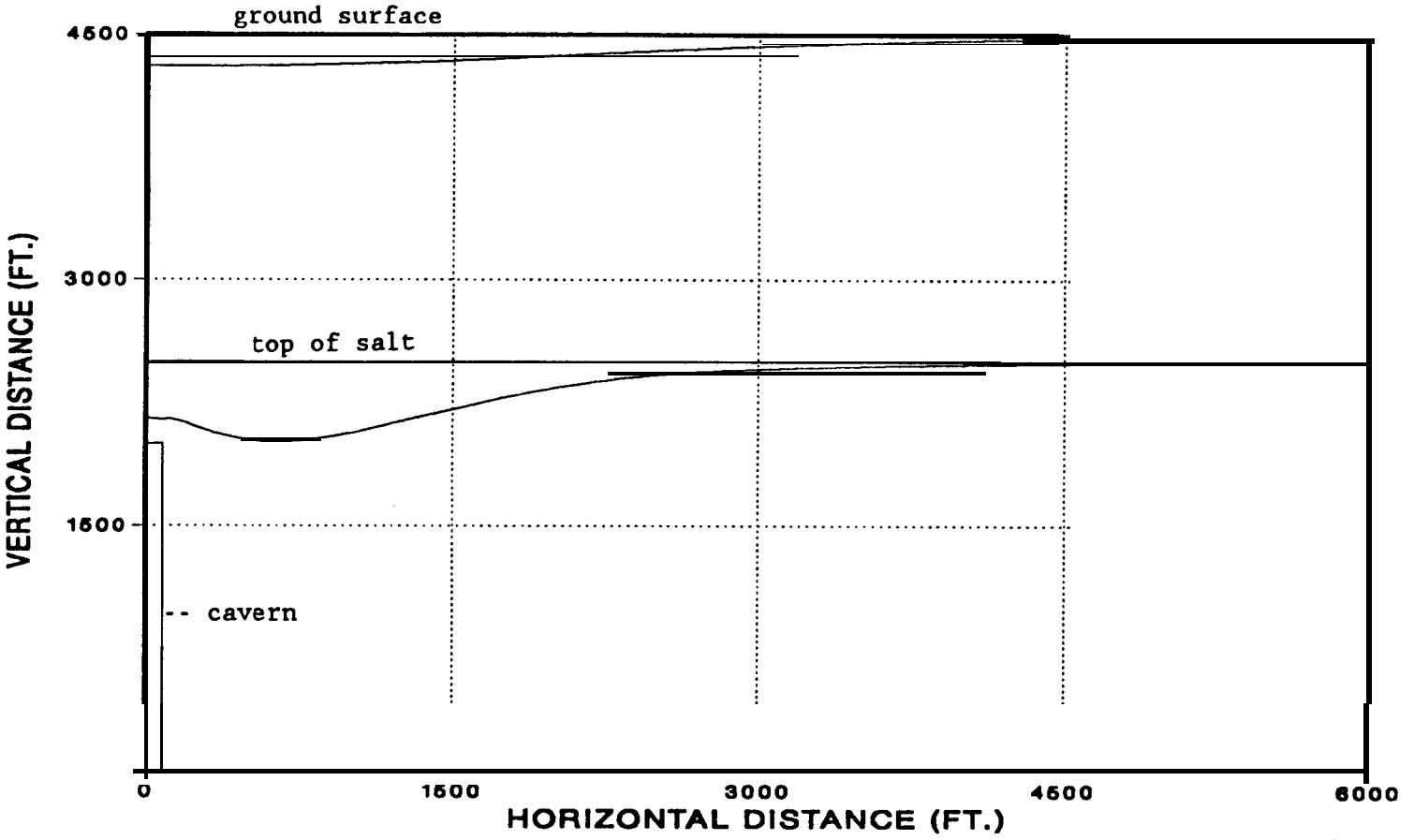

Figure 3. Subsidence Magnified 500 Times for an Isolated Unpressurized Cavern at 10 Years

Figure 4 plots the log of 30 year subsidence vs. log of cavern spacing. The resulting curve is nearly linear and can be fitted with the following approximation:

$$\text{subsidence(ft)} = 5.75\text{x}10^{9} \times (\text{spacing(ft)})^{-2.96}$$

where subsidence and spacing have units of ft. The correlation coefficient equals 0.998 resulting in a maximum error of 20 percent when compared to the code predicted results.

Figure 5 plots the subsidence vs. time curves for each of the cavern spacings modeled. The magnitude of the subsidence axis is adjusted on each of the subplots to provide a better view of the individual curves. Each of the curve shapes are similar in that a steady state response follows a transient portion of the curve. What differs is the duration of the transient response. The 375 ft. cavern spacing shows the transient occurring out to approximately 7 years, the 3000 ft. cavern spacing results in a much longer transient response-- perhaps beyond 30 years. This is most likely a result of the greater volume of salt, which allows the transient response to propagate farther and hence longer. Therefore closely spaced caverns are predicted to approach steady state subsidence faster than caverns separated farther, isolated, or perhaps at the edge of a field of caverns.

Figure 6 plots subsidence vs. time on a log plot for each of the 4 spacings modeled. The initial subsidence shown in the figure is at 1 day, as the log of a zero number is not permitted. This plot shows orders of magnitude difference in the predicted subsidences.

Figure 7 plots the subsidence rates over 30 years for the 4 cavern spacings modeled. The rates, similar to the predictions of subsidence, vary by orders of magnitude over the various cavern spacings. The plot shows steady state subsidence as a horizontal line.

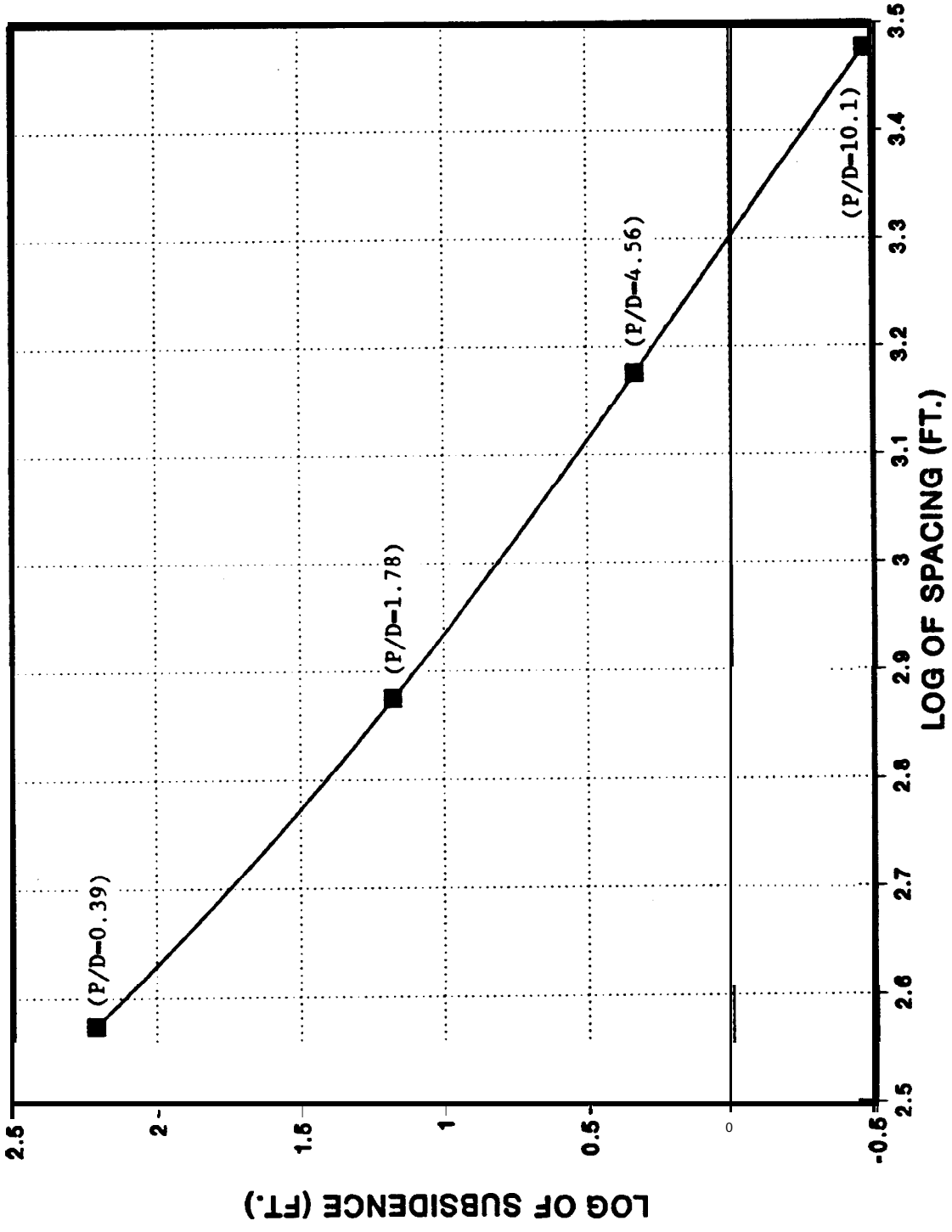

Figure 4 Subsidence at 30 Years vs. Cavern Spacing.

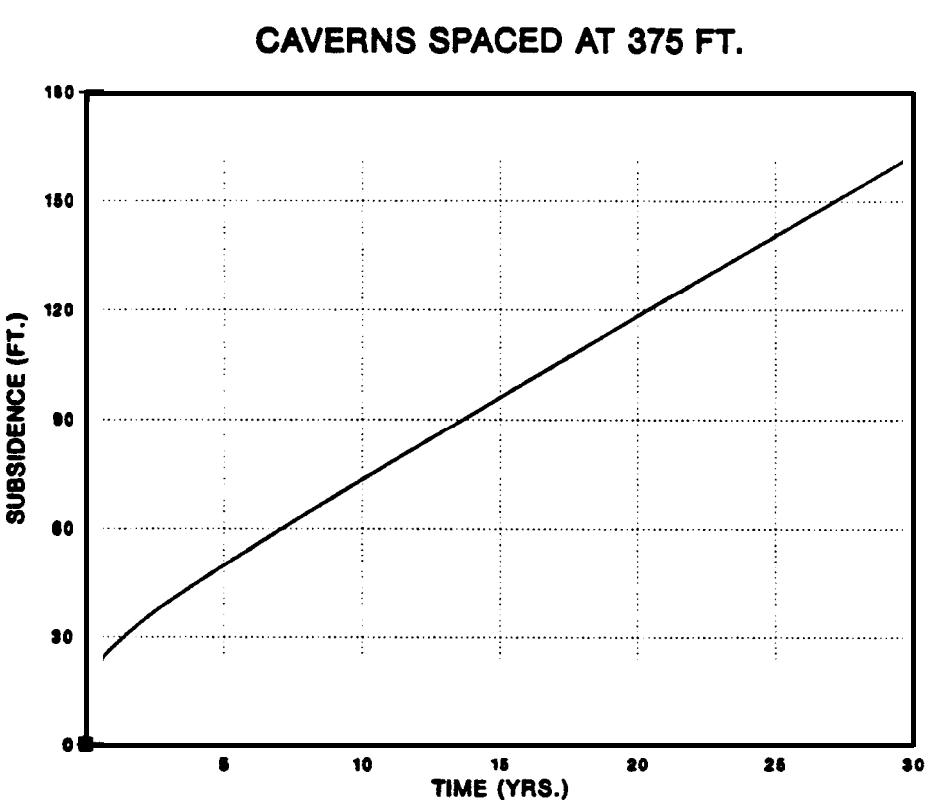

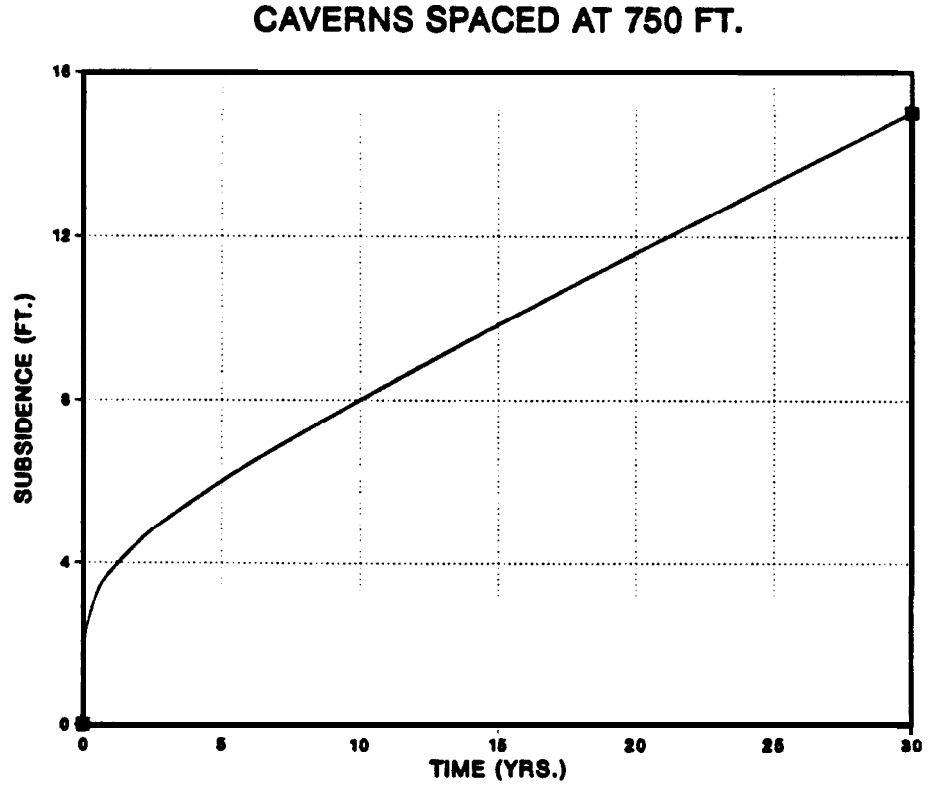

Figure 5. **Subsidence vs.** Time for Caverns **Spaced** at 375, 750, 1500, and 3000 **ft.**

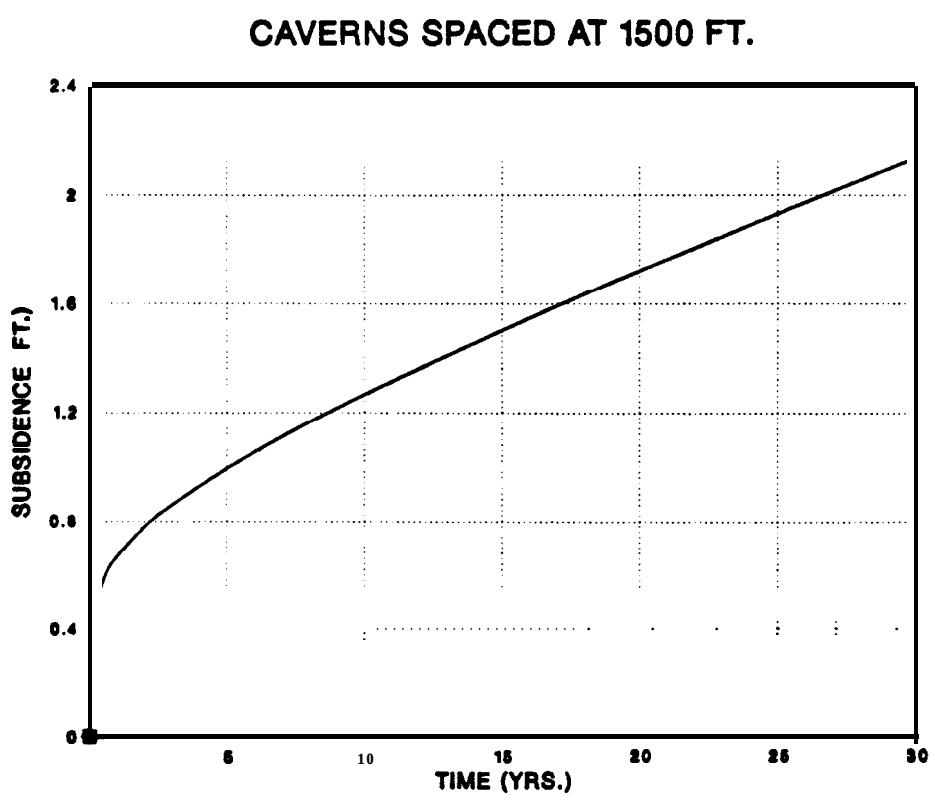

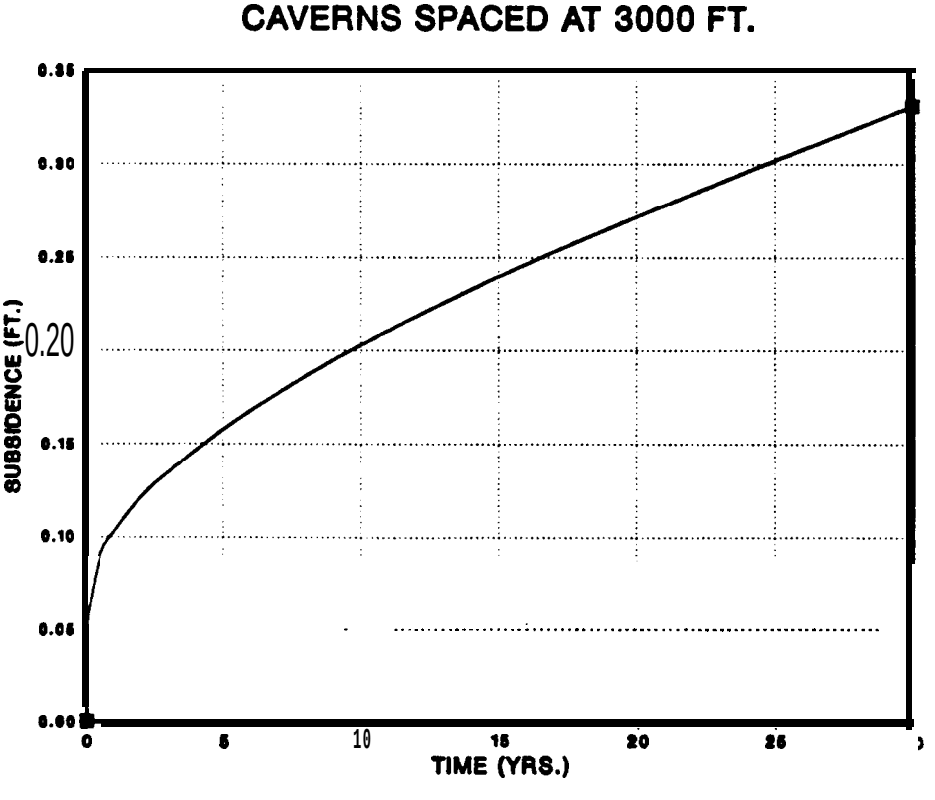

Figure 5 (Continued). Subsidence **vs.** Time for **Caverns** Spaced at 375, 750, 1500, and 3000 ft.

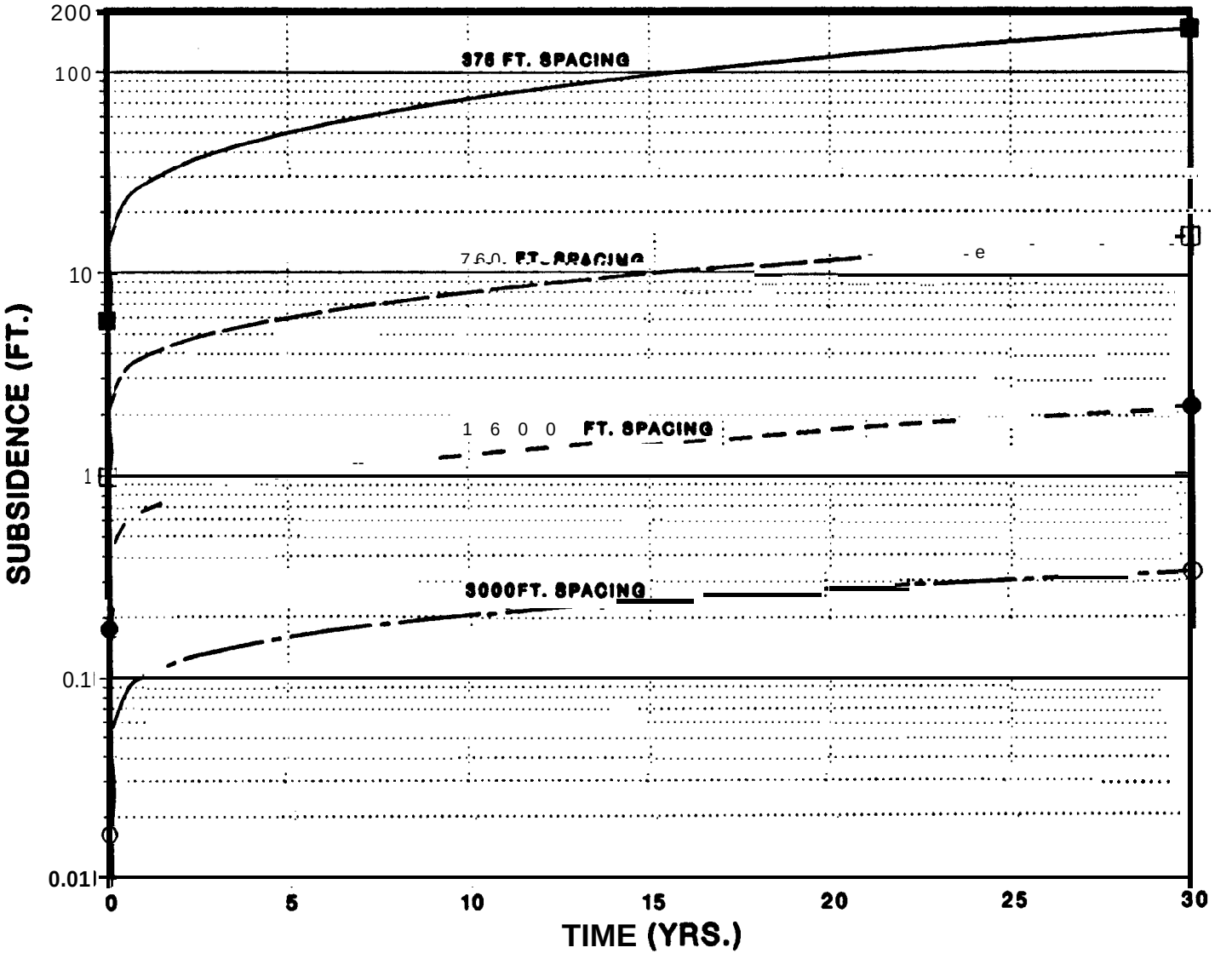

Figure 6. Subsidence vs. Time for Caverns Spaced at 375, 750, 1500, and 3000 ft. (Semi-Log Plot).

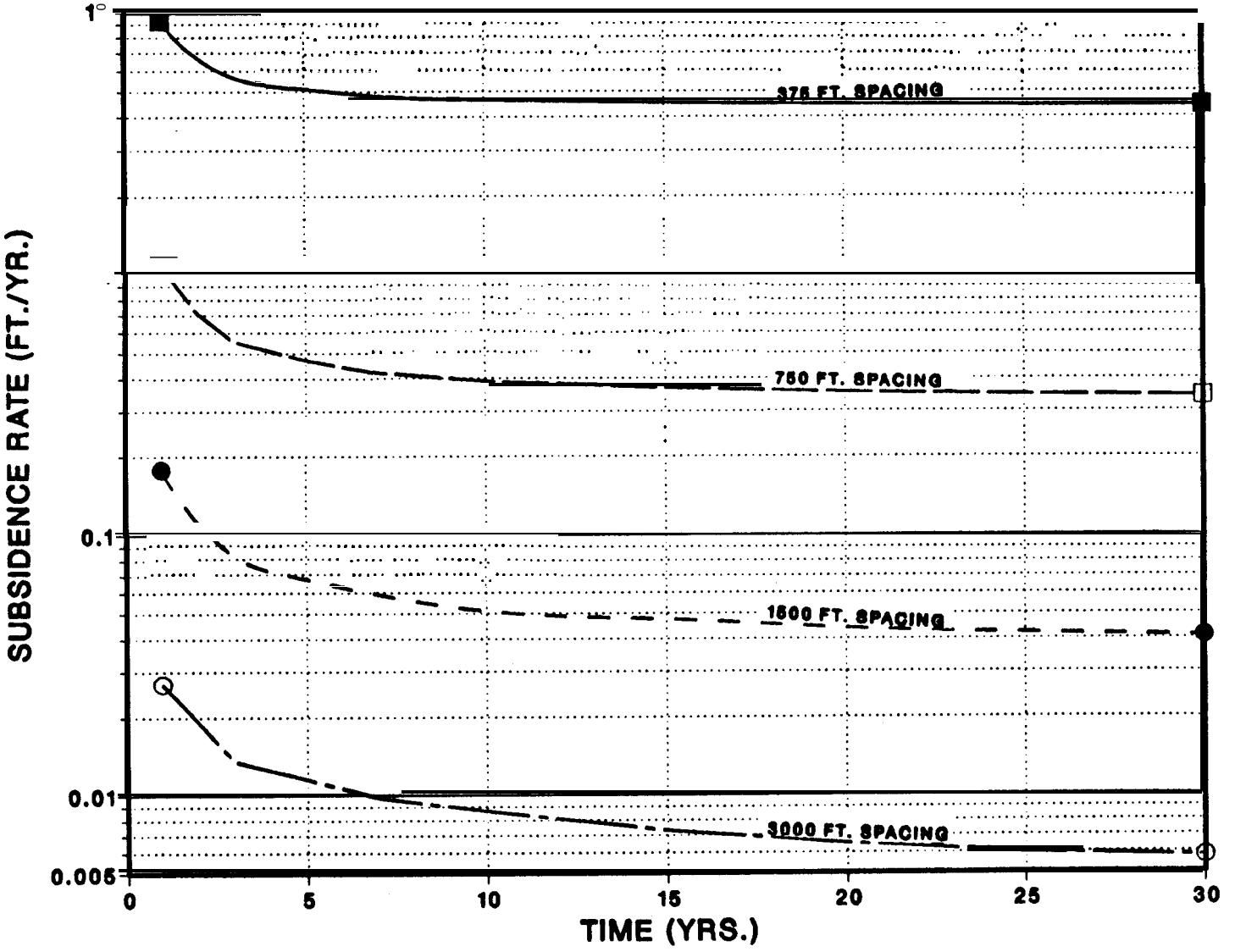

Figure 7. Rate of Subsidence vs. Time for Caverns Spaced at 375, 750, 1500, and 3000 ft.

4.2 Effects on Storage Loss

Figure 8 shows the predicted relationship between cavern spacing and cavern volume losses at 30 years. The loss of cavern volume is due to creep, and approximately 50 percent of the volume losses occur within the bottom 20 to 25 percent of the cavern. The relationship between spacing and cavern loss is not nearly as strong as it was with subsidence.

Figure 9 plots the volume loss as a function of time for each of the 4 cavern spacings modeled. In all cases an abrupt transient response is predicted by the model within the first year. Because the caverns were modeled as instantaneously mined, the initial results may not accurately represent actual cavern behavior where solution mining typically requires approximately 2 years to complete a cavern. Actual transients will not occur as abruptly, but will be more evenly distributed over the solution mining time.

Figure 10 plots the rate of volume loss over 30 years for each of the 4 cavern spacings modeled. The rate of volume loss does not become constant in time for any of the spacings modeled. Therefore, volume losses do not reach steady state as the rates are continuing to decrease with time. This is in contrast to subsidence, which is predicted to reach steady state within 30 years (Figure 7).

Figure 11 plots the deformed cavern shapes at 30 years for each of the 4 spacings. Cavern deformation is greatest at a distance of approximately 7 to 10 percent of the cavern length up from the floor. The volumes lost due to upheaval of the floor were relatively insignificant when compared to overall cavern losses. The dominant reason for storage loss in all cases was due to wall closure, although cavern shortening (primarily through lowering of the roof) was increasingly important for the smaller cavern spacings. For example, 27 percent of the total cavern loss was due to cavern shortening when the caverns were modeled at a spacing of 375 ft. For the smaller cavern spacings, the amount of roof subsidence is nearly equal to surface subsidence. This implies that the rock above the cavern translates in rigid body motion over

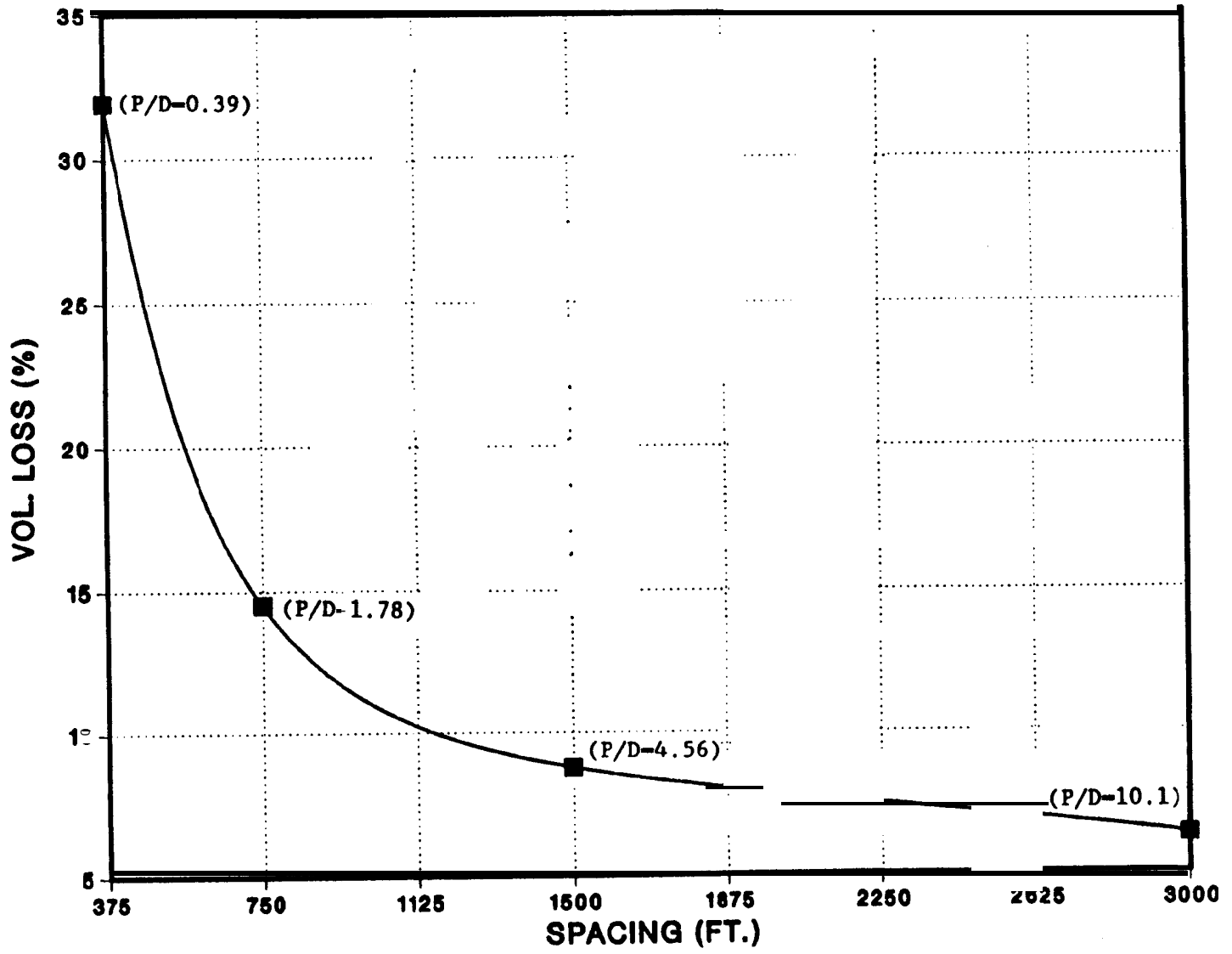

Figure 8. Cavern Storage Losses at 30 Years vs. Cavern Spacing.

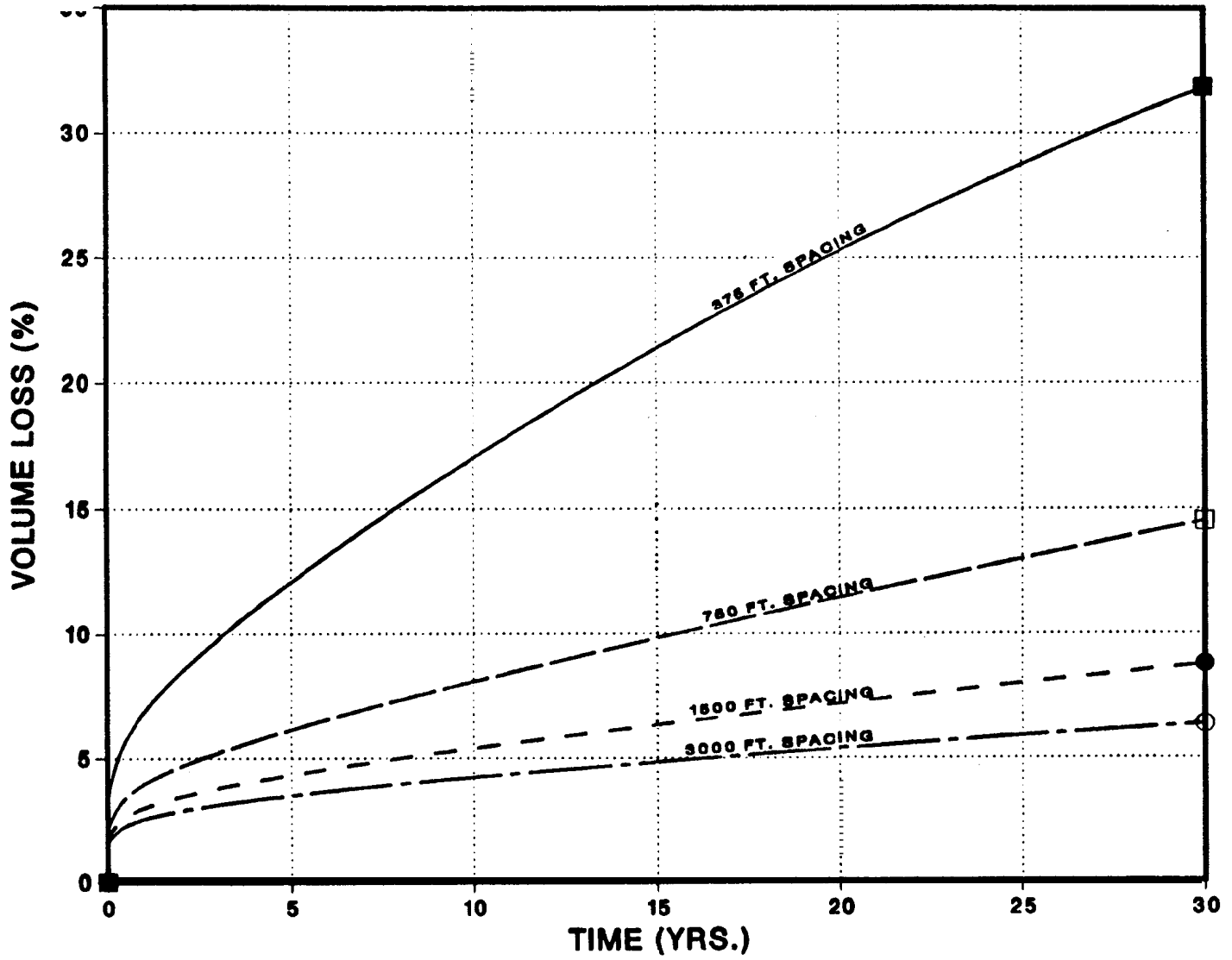

Figure 9. Cavern.Storage Losses vs. Time for Caverns Spaced at 375, 750, 1500, and 3000 ft.

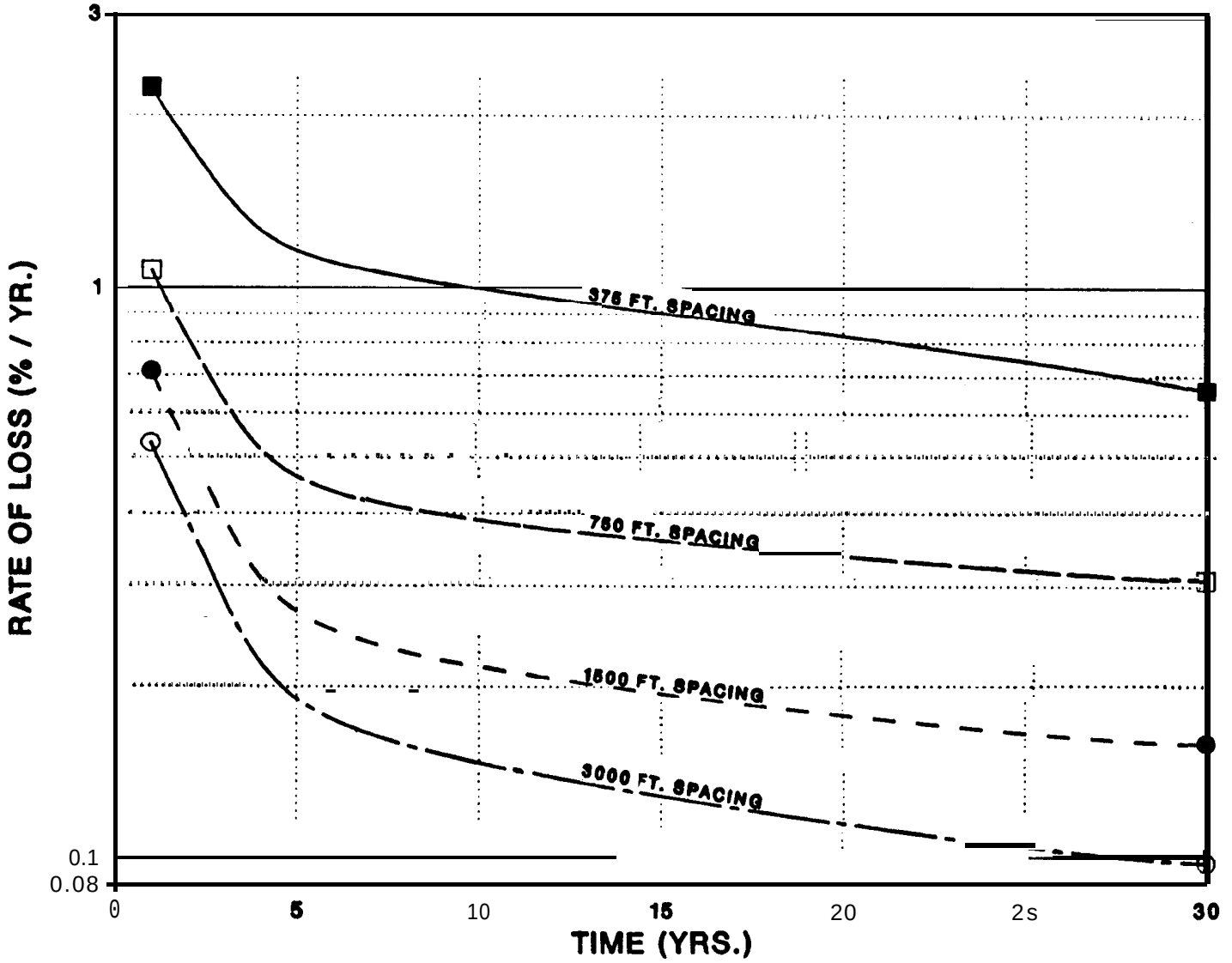

Figure 10. Rate of Cavern Storage Losses vs. Time for Caverns Spaced at 375, 750, 1500, and 3000 ft.

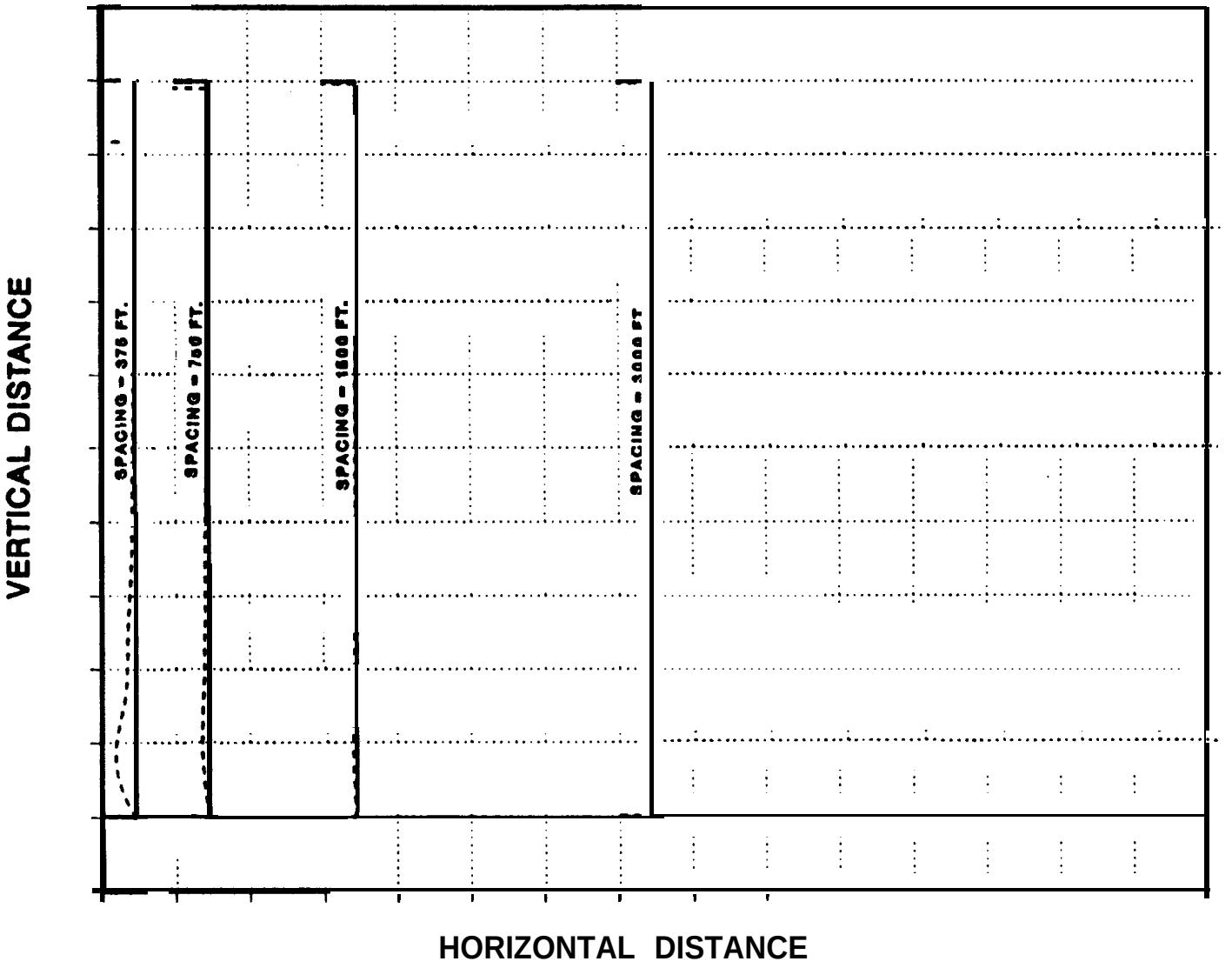

Figure 11. Cavern Deformations at 30 Years for Caverns Spaced at 375, 750, 1500, and 3000 ft. Because of symmetry only one-half of cavern is shown.

time. As a result, strains accumulated in the rock directly above the cavern are limited.

4.3 Cavern Integrity

The stability of the caverns was evaluated using a strain accumulation failure model for the salt. The model has been used for WIPP (Krieg, 1984; Munson, 1989) and SPR (Preece and Wawersik, 1984) salt and is based on triaxial laboratory tests on salt. For the mean pressures predicted near the locations of greatest deformation, the criteria predicts stability when the accumulated creep strain is below 13.8 to 15.5 percent. Failure was possible in the wall near the bottom of the closest spaced cavern (375 ft.). At this location, the wall bulges into the cavern (Figure 11) resulting in a diametrical closure of approximately 60 percent.

Isolated areas of salt fracturing do not necessarily result in overall cavern failure. Further, the predictive model does not account for the possibility of fracture healing. Thus, the predicted fracturing is interpreted as a caution, and additional stability evaluations are recommended before caverns are spaced closer than the 750 ft. baseline. The caverns spaced at 750, 1500, and 3000 ft. were predicted to be stable.

For all spacings analyzed, the maximum strain in the region between the roof of the cavern and ground surface is small (< 0.01%) and should not result in structural yield of a steel casing. The deepest casing is typically set at 100 ft. above the roof of the cavern.

5.0 ANALYTICAL RESULTS OF CAVERN PRESSURIZATION STUDY

The effects of cavern operating pressure on surface subsidence and cavern storage or volume losses are discussed together, rather than separately as in the previous chapter, to better understand their inter-relationship with cavern pressure.

5.1 Effects on Subsidence and Storage Loss

Figure 12 plots the histories of subsidence and storage volume losses for the 4 oil side pressures analyzed, i.e., 0, 300, 680, and 1050 psi. The baseline oil pressure was 680 psi at the wellhead. All of the calculations used a cavern spacing of 750 ft. Similar to the results of the cavern spacing study, the predicted subsidence contours at the surface are essentially flat over time for all of the pressures simulated. In Chapter 4, a single isolated cavern simulated at 0 psi oil side pressure resulted in a subsidence trough. It appears that both cavern spacing and pressurization must depart from baseline values before a subsidence trough can be predicted. The edge of a cavern field may be analogous to an area where there are transitions in both cavern spacing and pressure.

A rule of thumb emerges from the analytical predictions. If storage losses are less than 20 percent, the volume of storage loss is roughly equal to the volume of surface subsidence. When expressed in ft., subsidence is approximately equal to the percentage of storage loss. This implies that volume reduction in the cavern is directly manifested as subsidence volume at the surface. Differences may exist between subsidence volume and the volume lost in the cavern because of accumulated strains in the salt, caprock, or overburden.

Figure 13 plots subsidence and storage loss as a function of well pressure at 5, 10, and 30 years. As expected, the trends show that both subsidence and storage losses decrease with increased cavern pressures.

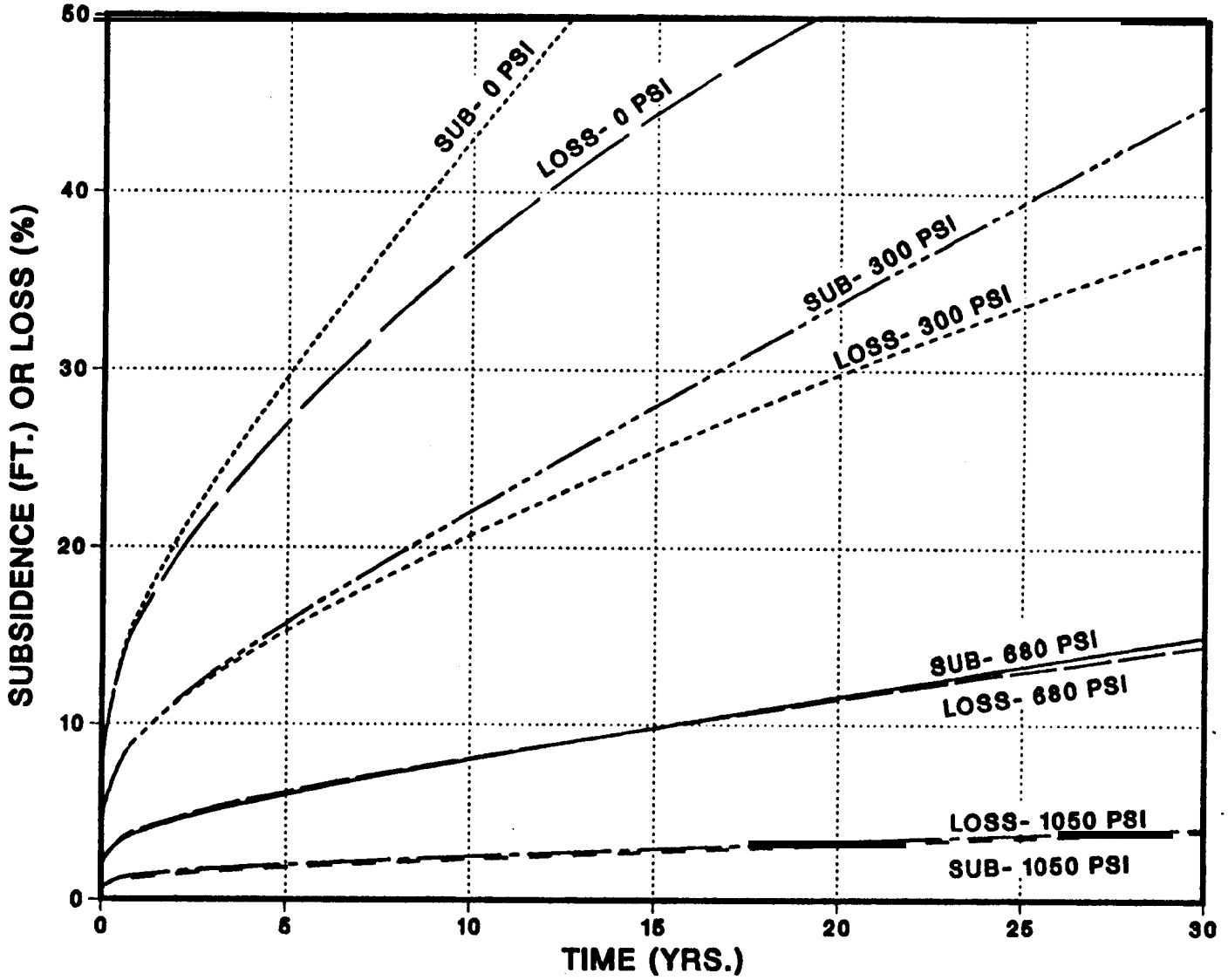

Figure 12. Subsidence or Cavern Storage Losses vs. Time for Cavern Oil Pressures of 0, 300, 680, and 1050 psi.

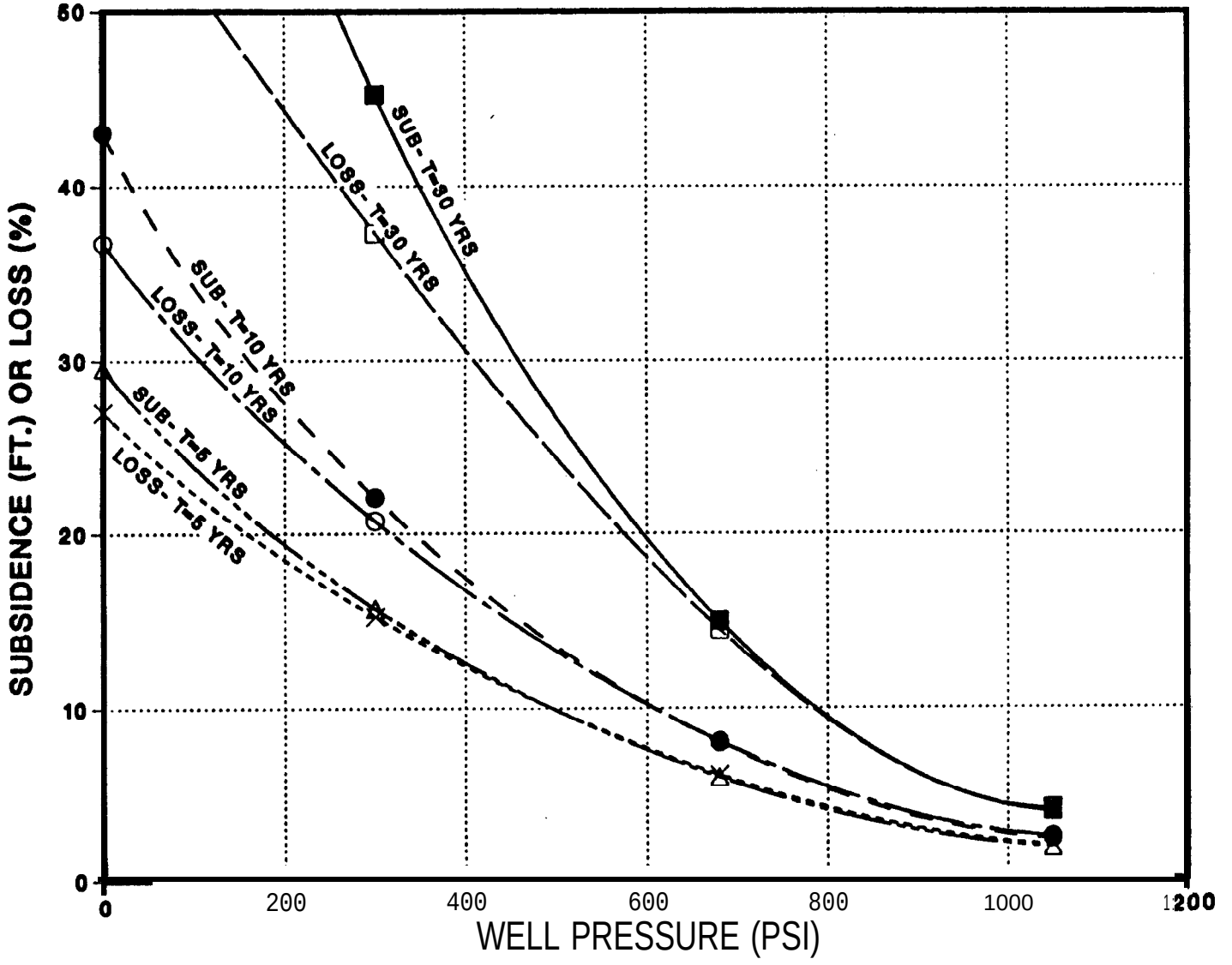

Figure 13. Subsidence or Cavern Storage Losses vs. Cavern Oil Pressure at 5, 10, and 30 Years.

The decreases in subsidence and storage losses lessen as the cavern approaches its maximum operating pressure (1050 psi). Figure 13 can be used as a design or operating tool to help establish a desirable cavern operating pressure for a typical SPR cavern.

Figure 14 shows the log of subsidence and storage loss versus well pressure at 5, 10, and 30 years. A linear fit to the results at 30 years, yield the following relationships for a typical SPR cavern.

$$\text{subsidence(ft)} = 103 \times 10(-0.00131 \times \text{pressure(psi)})$$

and

$$\text{storage loss(\%)} = 69.5 \times 10(-0.00111 \times \text{pressure(psi)})$$

Subsidence, pressure of the oil side, and storage loss have units of ft., psi, and percent, respectively. The curve fits represent the predicted subsidence or storage loss to within 20 percent.

Figure 15 shows profiles of cavern deformations at 30 years for 0, 300, 680, and 1050 psi oil side pressures. At 0 psi well pressure, the cavern is 59.2 percent closed at 30 years. Note the walls are in contact over the lower portion of the cavern exclusive of a small area at the very bottom of the cavern. This area would be completely encapsulated in salt. The walls of the cavern contact each other at approximately 25 years into the 0 pressure simulation. For the 0 pressure simulation, 93 ft. of subsidence is predicted at the surface after 30 years. Similar to the spacing study, the subsidence or vertical displacement predicted in the roof of the cavern is approximately equal to the predicted surface subsidence. For the other pressure cases (300, 680, and 1050 psi), the profiles for wall displacements are similar to the 0 psi case, but significantly reduced in magnitude.

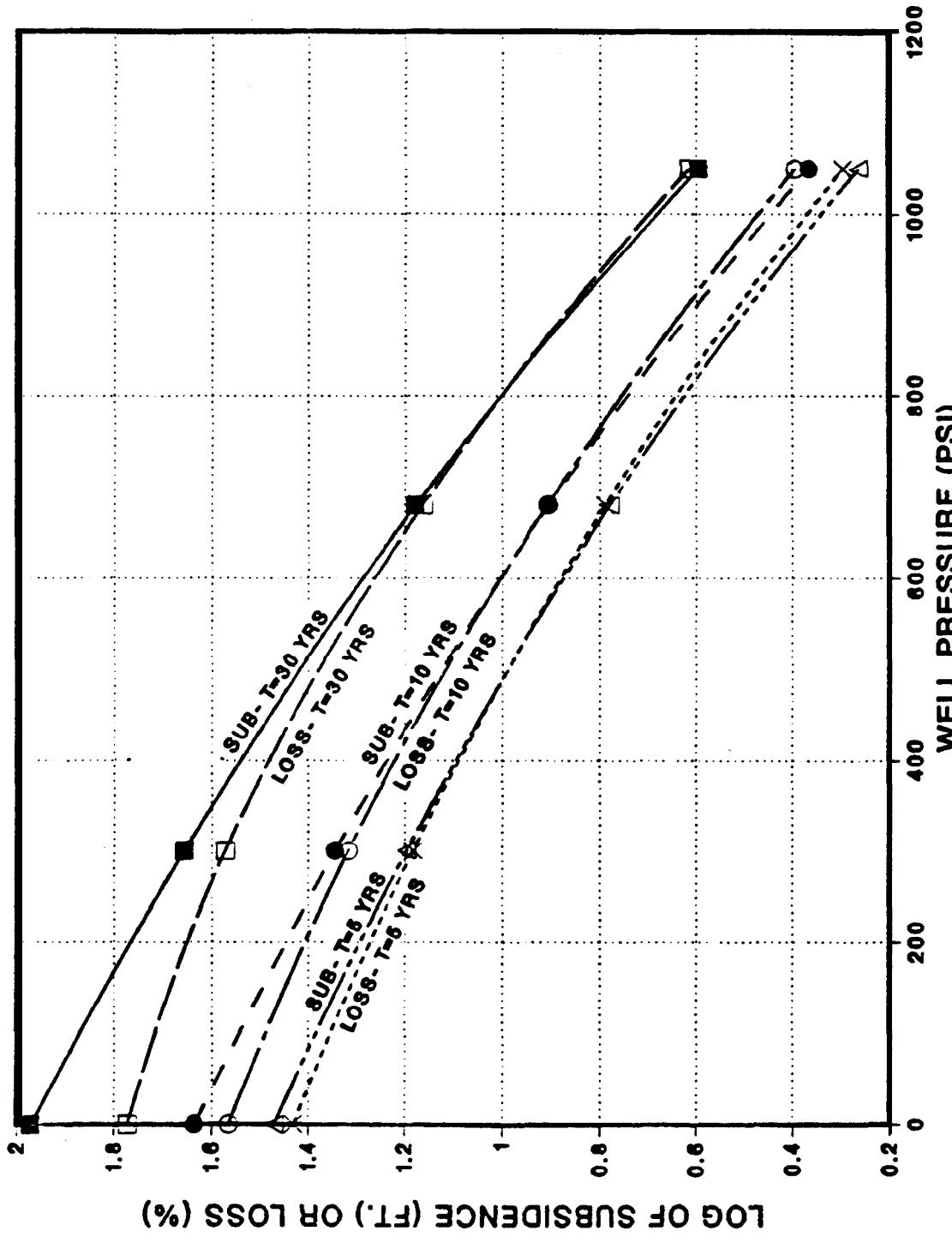

Figure 14. Log of Subsidence and Cavern Storage Losses vs. Cavern Oil Pressure at 5, 10, and 30 Years.

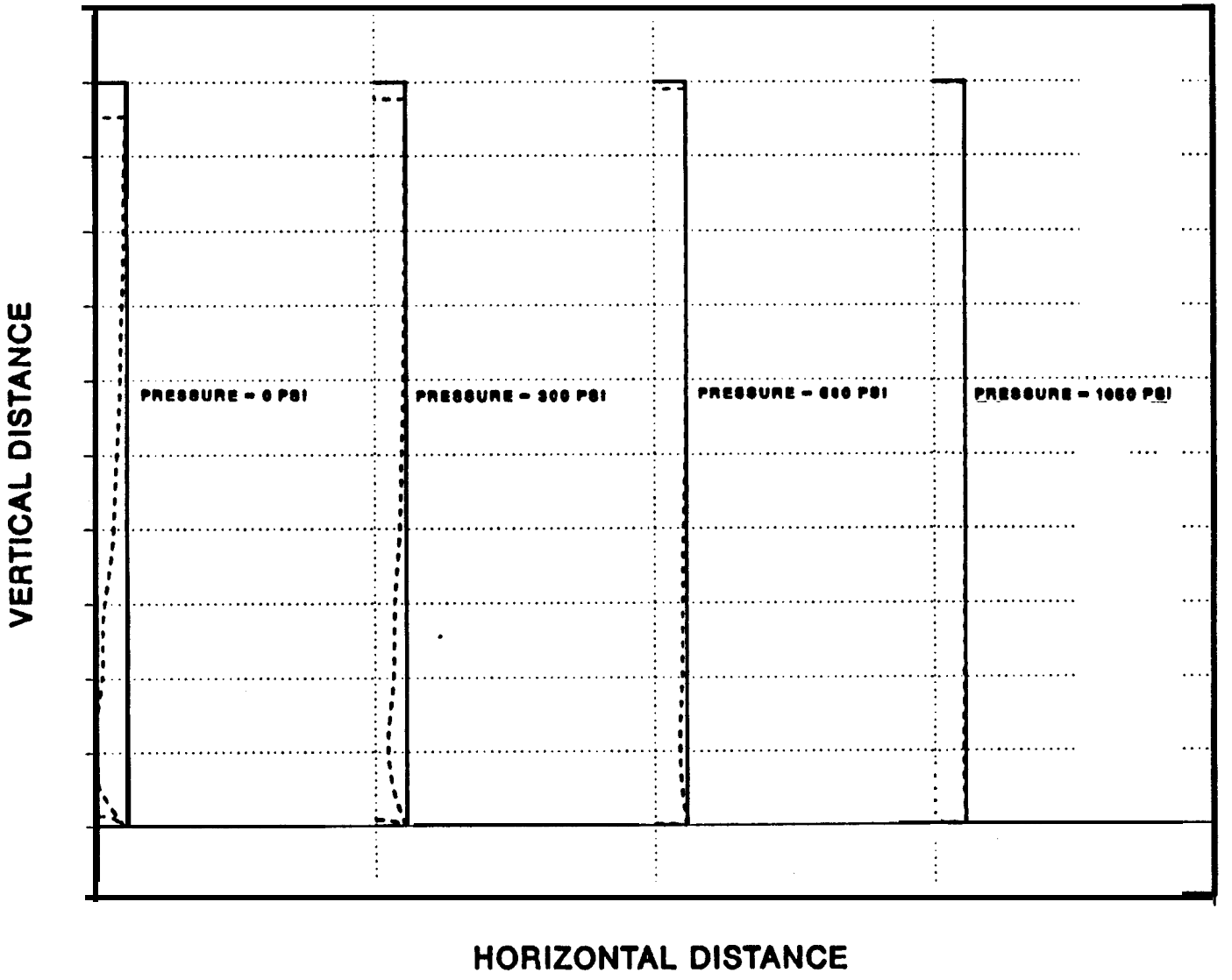

Figure 15 Cavern Deformations at 30 Years for Well Pressures of 0, 300, 680, and 1050 psi.

5.2 Cavern Integrity

All of the caverns are predicted to be stable using the previously discussed stability criterion (Chapter 4). In the case of the 0 psi cavern, a localized portion of the wall near the bottom of the cavern is predicted to be at the limit of the stability criterion at 30 years; however, that area is also predicted to be closed so fracturing would be of no consequence, if it were to occur.

Similar to the results of the cavern spacing study, the amount of elongation between the cavern roof and ground surface is small and should not result in structural yield of the casing. The predicted differential strain over the length of the casing is small despite relatively large subsidence predictions because the rock above the cavern subsides in a fairly rigid body motion.

6.0 COMPARISON OF PREDICTED RESULTS TO FIELD MEASUREMENTS

The modeling approximations and assumptions can be checked by comparing modeling predictions of the base case (typical SPR cavern) to field measurements of subsidence and cavern pressures. In addition, the results of the pressurization study can be compared to cavern pressurization data, as the caverns typically operate over a range of pressures.

First, the predicted subsidence profiles and storage losses can be compared to general site observations. The predicted shape of the subsidence profile from the cavern spacing and pressurization analyses was uniform with no subsidence trough formed across the surface. At the SPR sites, measured subsidence undulates across the surface of most cavern fields (Goin and Neal, 1988), but overall appears to be relatively uniform. The undulations may be a result of survey inaccuracies, geologic inhomogeneities, and different cavern operating histories. However, subsidence measurements are limited to the cavern fields. Measurements beyond the edge of the property boundaries may be necessary in order to detect a subsidence profile. An exception is at West Hackberry where a distinct subsidence trough is formed within the cavern field. In regards to storage loss, a prevalent rule of thumb estimates cavern losses to be on the order of 10 percent in 30 years. For the typical SPR cavern, the modeling results predict a 30 year loss of 14.5 percent. If the predicted volume losses (based on instantaneous solutioning) within the first year are excluded to account for the realities of a gradual solution mining process, the volume losses are predicted to be 11.1 percent at 30 years. The corresponding prediction for surface subsidence is 11.2 ft. at 30 years.

6.1 Subsidence Rates

More detailed comparisons can be made with the measurements of subsidence rates at SPR West Hackberry because the material properties, cavern geometries and depths, and stratigraphy used in these analyses

closely approximate or were derived from data from that site.

Subsidence measurements (Goin and Neal, 1988; McHenry, 1989) for caverns 107 and 115 are reported in Table 3. Caverns 107 and 115 are centrally located caverns in a field of 22 caverns total. Neighboring caverns are located at approximately 750 ft. Cavern 107 has 5 neighbors, whereas 115 has 6 neighbors.

Table 3
Measured Subsidence at West Hackberry Caverns 107 and 115

Date	1/83	8/83	2/84	3/85	9/86	12/87	12/88
Cavern 107:							
Elev. above sea level (ft.)	15.84	15.73	15.50	15.15	14.75	14.47	14.41
Sub. Rate (ft./yr.)		.189	.460	.323	.267	.224	.060
Cavern 115:							
Elev. above sea level (ft.)	9.15	9.07	8.87	8.43	8.03	7.72	7.62
Sub. Rate (ft./yr.)		.137	.400	.406	.267	.248	0.10

Solution mining of caverns 107, 115, and their neighbors generally commenced mid 1981 to early 1982, with completion and filling with oil some 3 years later.

Both sets of subsidence data exhibit similar trends in which the rate of subsidence increases to a maximum value (which corresponds to the time when most of the solutioning was complete) and then decreases.

The cavern simulations only exhibit a decrease in the subsidence rate because each cavern in the simulation was created instantaneously and at the same time. Furthermore, the model assumes an infinite array of caverns, whereas actual cavern fields are of finite extent. The edge effects of the field will produce less storage loss and subsidence. Therefore the predicted subsidence rates are expected to be greater than those measured above a cavern field of finite extent, gradually brought into existence. In general, the predicted subsidence rates that correspond to the above dates decrease from 1.1 to 0.45 ft/yr. Given the modeling assumptions, the predicted subsidence rates are reasonable when compared to the measured values.

6.2 Cavern Pressurization Rates

Another metric of cavern behavior is the measured oil side pressure at the wellhead. Because of creep and thermal effects, the oil in the cavern pressurizes with time. Periodically, the pressure is bled to form the start of a pressure cycle. Cavern pressurization data (Cavern Pressurization Report, 1990) for Caverns 107 and 115 are listed in Table 4 for the previous 2 years. Cavern 107 pressures for early 1991 are not listed as the cavern underwent a workover during that period. The 2 year period represents a relatively inactive period for the caverns.

Although not as obvious, as in the subsidence data, the cavern pressurization rates appear to be decreasing over the 2 year period, exhibiting relatively minor fluctuations. The data show the caverns to be pressurizing at a rate of approximately 1.8 to 2.0 psi/day.

Neglecting thermal effects (which cause higher pressurization rates), the simulated cavern pressurization rates can be calculated from the predicted storage loss rate. Thermal effects are assumed to be negligible as the caverns are approximately 6 years old. Estimating the compressibility of crude as 5.763-6 l/psi (API-37.5, P-2265 psi, T=125°F), the predicted pressurization rate from the modeling of a 6 yr old cavern is 2.01 psi/day. The predicted value agrees quite closely with the measured data.

A characteristic response of salt and consequently oil pressure following a pressure bleed is illustrated in Figure 16. Cavern depressurization loads the salt as creep is controlled by deviatoric stresses. Two components of the response are noted-- transient (ct) and steady state (ε_s). Transients accumulate to a maximum value (ε_t^*) which is known as the transient strain limit for salt. The corresponding oil pressure is defined simply as 'transient pressure' in this report. Steady state salt creep is linear resulting in a constant oil pressurization rate. The two components sum to form the total response of the cavern. The above characteristics are also described by Biringer (1987), who developed an empirical model for cavern pressurization.

The results of the cavern pressurization study can be compared to pressurization data collected at different average wellhead pressures. Pressure data from West Hackberry caverns 101, 107, and 110 were analyzed (Ehgartner, 1991) to determine (1) steady state pressurization rates as a function of average cavern operating pressure and (2) transient pressure responses as a function of bleed pressure. Caverns 101, 107, and 110 each have 5 neighboring caverns spaced approximately 750 ft. away.

Table 5 shows the data and results of the evaluation of pressure data for the caverns. Each row of data represents a pressure bleed. The transient pressure and steady state pressurization rate are observed from the data in accordance with the behavior described in Figure 16. The average cycle pressure is simply the average of the initial and final pressure (prior to bleed) in a cycle. Each pressure cycle is

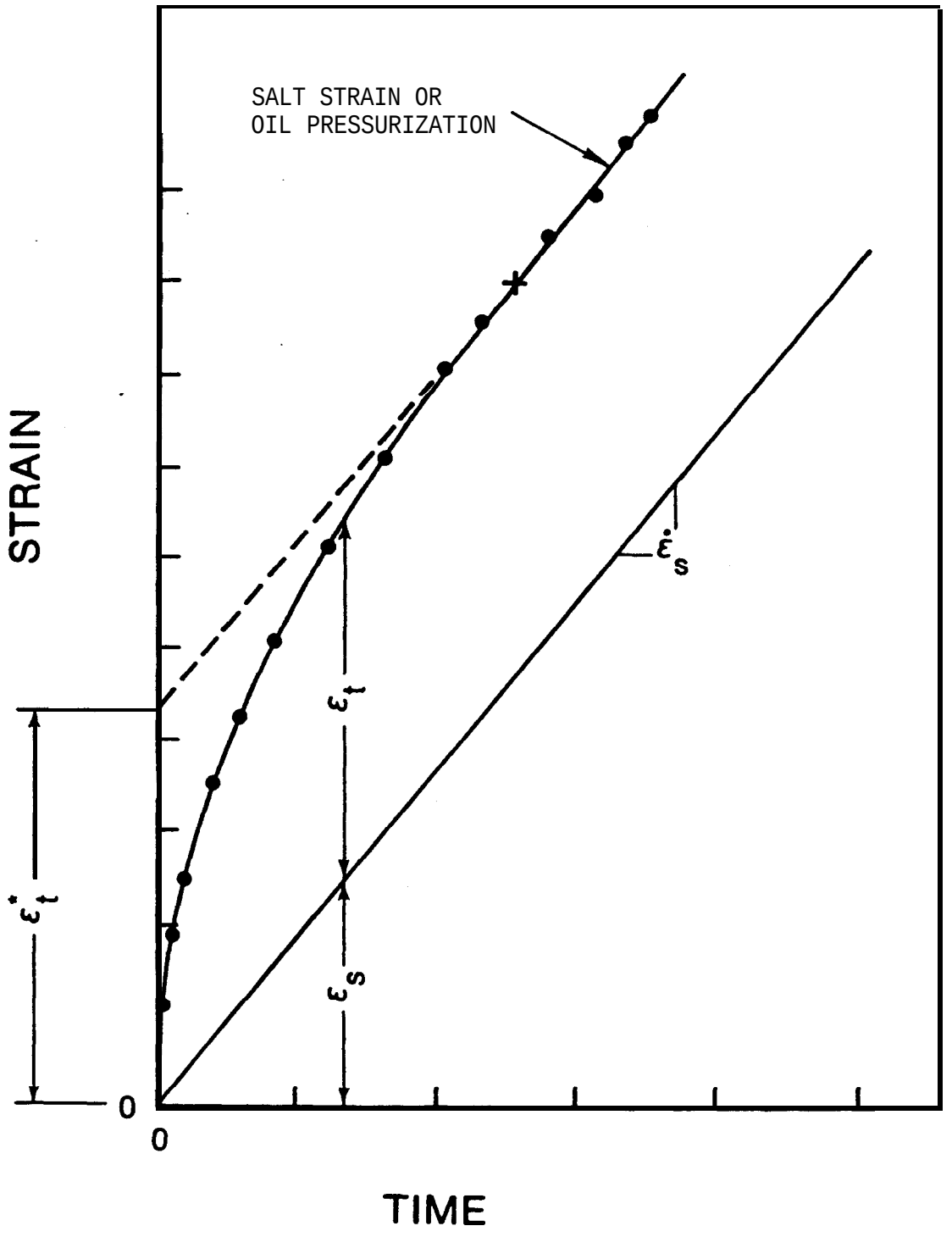

Figure 16. Typical Cavern Response Following Deprcssurization (after Munson, **Fossum,** and Senseny, 1989).

Table 5

Evaluation of West Hackberry Caverns

101, 107, and 110 Pressure Data

Date Depressurized	Bleed Pressure (psi)	Pressure Transient (psi)	Steady State Pressurization Rate	Average Cycle Pressure (psi)
Cavern 101:				
10/09/86	125	21	1.6	857
01/28/87	50	13	1.55	910
03/25/87	100	27	1.5	915
05/20/87	50	13	1.4	950
06/23/87	90	16	1.25	935
08/21/87	180	29	1.8	850
01/06/88	120	37	1.6	860
01/21/90	45	7	1.1	950
Cavern 107:				
12/18/86	85	22	1.5	930
03/09/87	125	30	1.1	927
08/21/87	145	34	1.6	832
09/04/89	145	29	1.7	942
11/01/89	70	22	1.5	970
01/24/90	75	33	1.2	970
03/21/90	90	26	1.4	972
05/03/90	105	34	1.0	940
05/30/90	60	27	1.3	960
07/26/90	80	37	0.9	970
Cavern 110:				
08/26/86	100	28	2.0	775
10/06/86	120	45	1.8	837
01/28/87	115	23	1.5	905
03/25/87	160	19	1.6	885
10/01/88	220	38	1.9	860
02/15/89	130	38	1.3	950
05/21/90	90	20	0.95	965

intended to represent periods of normal cavern operation, and therefore, periods of and immediately following irregular cavern pressures or fluid transfers were not evaluated. Also short pressure cycles and histories involving gauge problems, leaks, bad readings, etc. were not included.

The steady state cavern pressurizations as a function of average cycle pressure are plotted in Figure 17 along with the predicted pressurization rates at 2 and 6 years. These times approximately bound the dates over which the data was collected. Although some scatter exists in the data, the analytic predictions bound the pressure data and correctly show a trend where lower cavern operating pressures result in higher steady state pressurization rates.

Figure 18 plots the maximum pressure transient of oil as a function of the cavern bleed pressure. As expected, larger pressure drops result in larger transients. Although the relationship between the variables is probably non-linear, on average, the transient pressure response of the oil is approximately 30 percent of the pressure bleed. Typical pressure bleeds due to normal operations and workovers were not directly modeled in the simulations presented in this report. The transient effects were accounted for in the baseline model by using a constant simulation pressure (680 psi) approximately 30 percent less than the typical average operating pressure at West Hackberry.

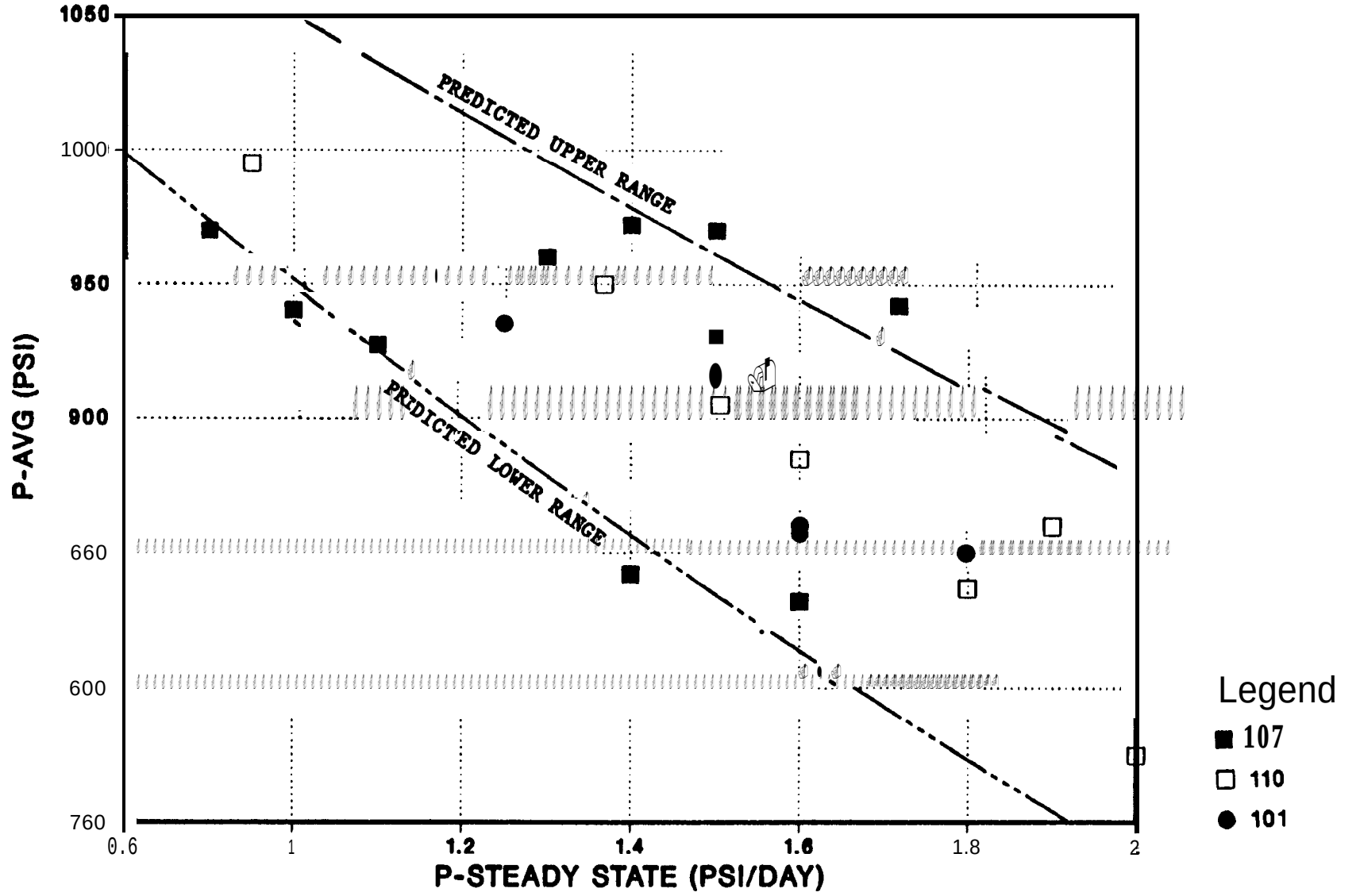

Figure 17. Steady State Oil Pressurization Rates of W.H. 101, 107, and 110 vs. Average Oil Side Pressure. Code predictions are also shown.

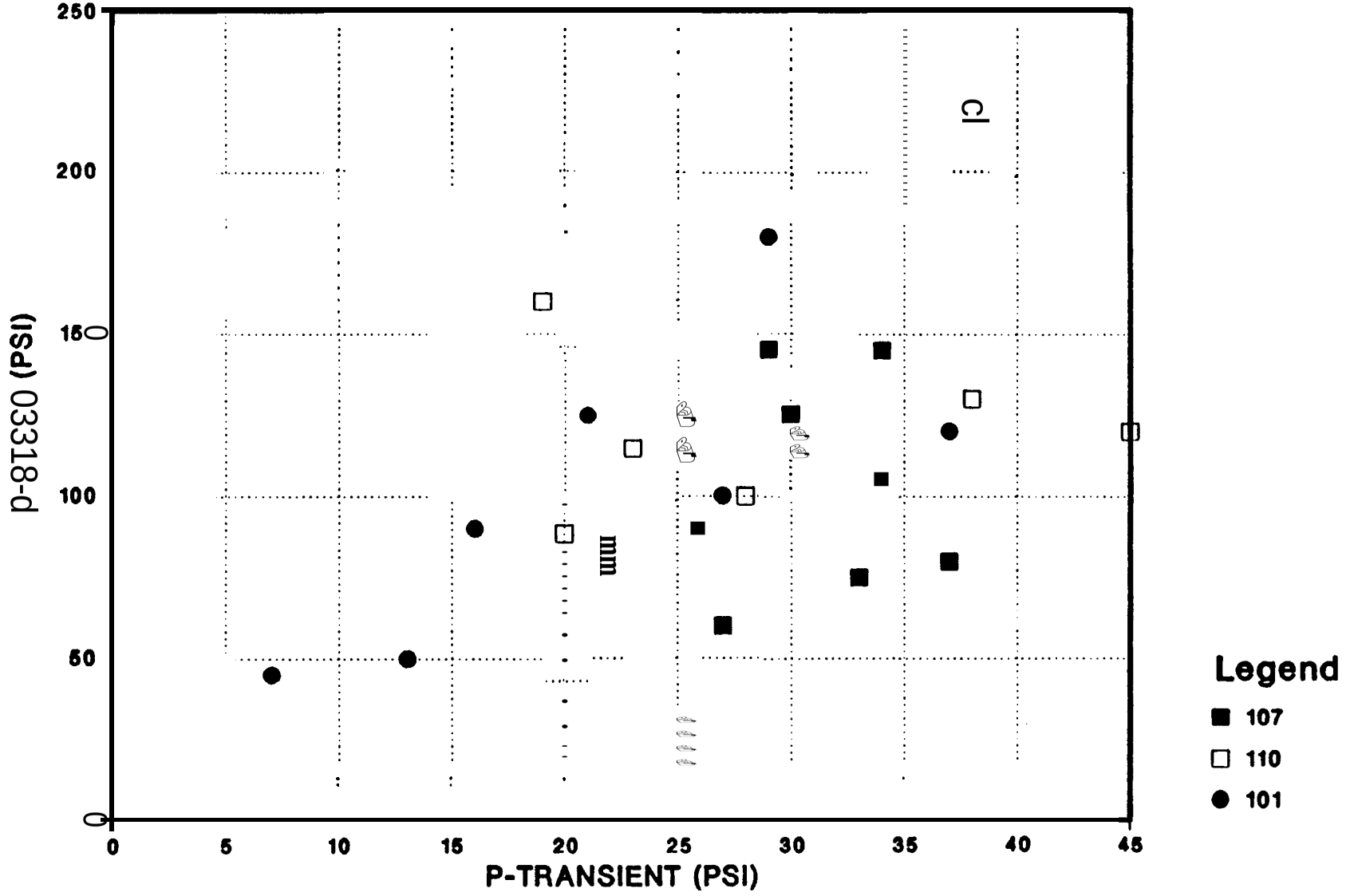

Figure 18. Oil Side Pressure Transients vs. Bleed Pressure for W.H. Caverns 101, 107, and 110.

7.0 CONCLUSIONS

The modeling results predict that cavern spacing strongly influences surface subsidence and moderately effects cavern volume losses. The cavern spacing study showed 30 year subsidence predictions to increase from 4 in. for a single isolated cavern to 162 ft. for closely spaced caverns at 375 ft. The corresponding storage losses ranged from 6 to 32 percent, respectively. Given the proximity of some SPR sites to sea level, the current minimum spacing criteria of 750 ft. appears prudent based on the subsidence predictions. Where subsidence is not an issue, a slightly closer cavern spacing may be possible if the increased rate of volume loss is tolerable and cavern stability is not a problem.

The results of the cavern pressurization study showed predicted 30 year subsidence to range from 4 to 93 ft. for oil side pressures from 1050 to 0 psi. Corresponding storage losses increased from 4 to 59 percent. The relationship between subsidence volume and losses in storage volume varied as cavern spacing and operating pressure deviated from the base case. However, for typical SPR cavern spacing and operating pressure, the predicted subsidence volume was proportional to storage loss and when expressed in ft., subsidence is equal to the percentage of storage loss. For example, after 30 years the typical SPR cavern is estimated to lose approximately 11 percent of its storage capacity, resulting in 11 ft. of subsidence. This analytical rule of thumb suggests that cavern volume losses are directly manifested as subsidence volume at the surface. Therefore, a dual penalty results (subsidence and storage loss) when caverns are operated at reduced pressures.

The results for the base case (typical SPR cavern spacing and operating pressure) and those of the pressurization study compare very well to subsidence and cavern pressurization rates measured in the field. Although model validation was not the focus of this report, the comparisons with field data suggests the model correctly predicts not only near-field (cavern) behavior, but far-field response (subsidence)

as well. This collaborates with the detailed model validation exercises in progress for the Waste Isolation Pilot Plant (Munson and **DeVries**, 1990).

Although the model used in this report is based on a typical SPR cavern, SPR caverns vary in shape, capacity, depth, spacing, number of caverns in a field, stratigraphy, operating pressures, etc. The salt characteristics for each dome varies as well. The analyses in this report most closely simulate the caverns at West Hackberry. However, the results are applicable in a qualitative sense to all SPR sites.

8.0 REFERENCES

Acres International 1986. Additional Geotechnical Studies Strategic Petroleum Reserve (SPR), SAND86-7181, Sandia National Laboratories, Albuquerque, NM.

Biringer, K.L. 1987. Strategic Petroleum Reserve (SPR) Long-Term Monitoring System Pressure Data Analyses, SAND87-0706, Sandia National Laboratories, Albuquerque, NM

Ehgartner, B.L. 1990. Geomechanical Analyses in Support of the Waste Isolation Pilot Plant (WIPP), SAND90-0285, Sandia National Laboratories, Albuquerque, NM.

Ehgartner, B.L. 1991. Structural Analyses and Design of a Concrete Liner that Limit the Disturbed Rock Zone Around Underground Openings in Salt;, SAND90-2702, Sandia National Laboratories, Albuquerque, NM.

Ehgartner, B.L. 1991a. "Analysis of Pressure Data from West Hackberry 101, 107, and 110", Internal technical memorandum to J. Todd, 9/13/91, Sandia National Laboratories, Albuquerque, NM.

Goin, K.L. and J.T. Neal, 1988. Analysis of Surface Subsidence of the Strategic Petroleum Reserve Crude Oil Storage Sites From December 1982 to January 1988, SAND88-1309, Sandia National Laboratories, Albuquerque, NM.

Krieg, R.D. 1984. Reference Stratigraphy and Rock Properties for the Waste Isolation Plant (WIPP) Project, SAND83-1908, Sandia National Laboratories, Albuquerque, NM.

McHenry, J.M. 1989. SPR Annual Subsidence Report Doc. No. D506-02291-09, Prepared for U.S. Dept. of Energy, New Orleans: LA.

Munson, D.E. 1979. Preliminary Deformation Mechanism Map for Salt (with Application to WIPP), SAND70-0076, Sandia National Laboratories, Albuquerque, NM.

Munson, D.E. 1989. "Proposed New Structural Reference Stratigraphy, Law, and Properties", Internal technical memorandum to distribution, 8/22/89, Sandia National Laboratories, Albuquerque, NM.

Munson, D.E. and P.R. Dawson, 1979. Constitutive Model for the Low Temperature Creep of Salt (with Application to WIPP), SAND79-1853, Sandia National Laboratories, Albuquerque, NM.

Munson, D.E. and K.L. DeVries, 1990. "Progress in Validation of Structural Codes for Radioactive Waste Repository Applications in Bedded Salt," Proc. of Geoval 90, Conference sponsored by SKI & OECD/NEA, Stockholm, Sweden.

Table 4

West Hackberry Caverns 107 and 115

Pressurization Data

Start Date	Start Pressure (psi)	Pressure Change (psi)	Cycle Duration (days)	Pressurization Rate (psi/day)
Cavern 107:				
09/05/89	885	75	25	3.00
11/02/89	930	80	39	2.05
12/22/89	900	95	33	2.88
01/25/90	920	100	55	1.82
03/22/90	930	85	43	1.98
05/04/90	910	60	27	2.22
05/31/90	910	100	56	1.79
07/27/90	930	80	49	1.63
10/02/90	910	85	50	1.70
				2.02 avg.
Cavern 115:				
09/15/89	920	70	27	2.59
11/30/89	670	155	63	2.46
02/15/90	750	100	49	2.04
05/20/90	725	105	44	2.39
07/04/90	920	90	67	1.34
09/10/90	980	20	17	1.18
09/28/90	900	110	74	1.49
12/14/90	940	60	31	1.94
01/22/91	910	110	60	1.83
03/28/91	910	140	89	1.57
06/28/91	920	80	52	1.54
				1.81 avg.

Munson, D.E., K.L. DeVries, D.M. Schiermeister, W.F. DeYonge, 1992. "Measured and Calculated Closures of Open and Brine Filled Shafts and Deep Vertical Boreholes in Salt," Proceedings of 33rd U.S. Symposium on Rock Mechanics, June 1992, Santa Fe, NM.

Munson, D.E., A.F. Fossum, and P.E. Senseny, 1989a. Advances in Resolution of Discrepancies Between Predicted and Measured In Situ WIPP Room Closure, SAND88-2948, Sandia National Laboratories, Albuquerque, NM.

Munson, D.E., A.F. Fossum, and P.E. Senseny, 1989b. Approach to First Principles Model Prediction of Measured WIPP In Situ Room Closure in Salt, SAND88-2535, Sandia National Laboratories, Albuquerque, NM.

Preece, D.S. 1984. Long-Term Performance Predictions for Strategic Petroleum Reserve (SPR) Salt Caverns, SAND83-2343, Sandia National Laboratories, Albuquerque, NM.

Preece, D.S. 1987a. 3-D Finite-element Calculation of Subsidence Induced Deformation of the Weeks Island Service Shaft, SAND87-2365, Sandia National Laboratories, Albuquerque, NM.

Preece, D.S. 1987b. Calculation of Creep Induced Volume Reduction of the Weeks Island SPR Facility Using 3-D Finite-element Methods, SAND87-1694, Sandia National Laboratories, Albuquerque, NM.

Preece, D.S. and W.R. Wawersik 1984. "Leached Salt Cavern Design Using a Fracture Criterion for Rock Salt," SAND83-2345C, Sandia National Laboratories, Albuquerque, NM. Also, Proceedings of 25th U.S. Symposium on Rock Mechanics, June 1984, Northwestern University.

RE/SPEC 1989. Documentation of SPECTROM-32: A Finite-element Thermomechanical Stress Analysis Program, RE/SPEC Inc., Rapid City, SD.

Senseny, P.E. 1990. Creep of Salt from the ERDA-9 Borehole and the WIPP Workings, SAND89-7098, Sandia National Laboratories, Albuquerque, NM.

SPR, 1987. Design Criteria- Level III, DOE U.S. Strategic Petroleum Reserve, New Orleans, LA.

Todd, J.L. personal communications, 1/23/91.

DISTRIBUTION

US **DOE** SPR **PMO** (5)
900 Commerce Road East
New Orleans, LA 70123
Attn: D. W. Whittington, PR-622
R. Myers, PR-622
L. Rousseau, FE-443
TDCS (2)

US DOE SPR (2)
1000 Independence Avenue SW
Washington, DC 20585
Attn: D. Johnson
D. Smith

Boeing Petroleum Services (3)
850 S. **Clearview** Parkway
New Orleans, LA 70123
Attn: K. Wynn
T. Eyerman
K. Mills

Boeing Petroleum Services (1)
1450 Black Lake Road
Hackberry, IA 70645
Attn: Jim Perry

Tejas Power Corporation (1)
14811 St. Mary's Lane
Suite 200
Houston, TX 77079
Attn: Greg Graves

Sandia Internal:

1514 H. S. Morgan
1514 E. L. Hoffman
6000 D. L. Hartley
6200 B. W. Marshall
6250 P. J. Hommert
6253 D. S. **Preece**
6257 J. **K.** Linn (10)
6257 S. J. Bauer
6257 B. L. Ehgartner (10)
6257 T. E. Hinkebein
6257 P. **S.** Kuhlman
6257 R. V. Matalucci
6257 J. T. Neal
6257 J. L. Todd
6257 S. T. Wallace
6346 D. E. Munson
8523-2 Central Technical Files
3141 S. A. Landenberger (5)
3145 Document Processing (8) for **DOE/OSTI**
3151 G. C. **Claycomb** (3)